DIRECT PATH INTERFERENCE SUPPRESSION AND RECEIVED SIGNAL PROCESSING FOR OFDM PASSIVE RADAR

THESIS

Aileen Nundu, FLTLT, RAAF

AFIT-ENG-MS-19M-049

DEPARTMENT OF THE AIR FORCE
AIR UNIVERSITY

AIR FORCE INSTITUTE OF TECHNOLOGY

Wright-Patterson Air Force Base, Ohio

AFIT-ENG-MS-19M-049

DIRECT PATH INTERFERENCE SUPPRESSION AND RECEIVED SIGNAL PROCESSING FOR OFDM PASSIVE RADAR

THESIS

Presented to the Faculty

Department of Electrical and Computer Engineering

Graduate School of Engineering and Management

Air Force Institute of Technology

Air University

Air Education and Training Command

in Partial Fulfillment of the Requirements for the

Degree of Master of Science in Electrical Engineering

Aileen Nundu, B.Eng

FLTLT, RAAF

March 21, 2019

AFIT-ENG-MS-19M-049

DIRECT PATH INTERFERENCE SUPPRESSION AND RECEIVED SIGNAL PROCESSING FOR OFDM PASSIVE RADAR

THESIS

Aileen Nundu, B.Eng
FLTLT, RAAF

Committee Membership:

Dr. J. A. Jackson
Chair

Dr. P. J. Collins
Member

Maj J. R. Lievsay, PhD
Member

Contents

Page

AFIT-ENG-MS-19M-049

Abstract

Passive bistatic radar (PBR) is a fairly active area of research due to the opportunities offered by the ability to use emitters of opportunity for target detection and tracking as well as Synthetic Aperture Radar (SAR) imaging. There is an increasing variety and availability of signals that can be exploited for passive radar and there is also the advantage of angular diversity offered by the bistatic geometry and the potential for stealth operations afforded a passive receiver. Notwithstanding its merits, PBR is complicated by the inevitable presence of Direct Path Interference (DPI) from the transmitter to the receiver, which can be orders of magnitude stronger than the echo signals from the targets of interest, resulting in missed targets. In addition, available signals are characterized by features necessary for the purpose for which they are designed, but that are not suited to radar applications due to the introduction of ambiguities in range and Doppler that mimic real targets. This thesis seeks to articulate two specific challenges of PBR in the context of SAR imaging using OFDM signals - DPI and range ambiguities, and the signal processing necessary to mitigate their effects. MATLAB® simulated scenarios are used throughout the work to illustrate the problem and solutions.

Acknowledgements

I thank my mother, whose unwavering support from thousands of miles away saw me through my degree, and whose sacrifices paved the way for me to be here at AFIT.

I am sincerely grateful to my thesis advisor, Dr. Julie Ann Jackson, for her insightful guidance throughout my time at AFIT. Her patience and much needed support made this thesis possible. I thank my committee members, MAJ J. R Lievsay and Dr. P.J. Collins, for their understanding and support in bringing my work together under challenging circumstances.

List of Acronyms

AF	Ambiguity Function
AWGN	Additive White Gaussian Noise
CAF	Cross Ambiguity Function
CP	Cyclic Prefix
CSRE	Cell-Specific Reference Elements
DAB	Digital Audio Broadcasting
DL	Downlink
DPI	Direct Path Interference (also DSI)
DSI	Direct Signal Interference (also DPI)
DVB	Digital Video Broadcasting
ECA	Extensive Cancellation Algorithm
EM	Electromagnetic
FBLMS	Fast Block Least Mean Squares
FDD	Frequency Division Duplexing
GSM	Global System for Mobile Communications
LMS	Least Mean Squares
LS	Least Squares
LTE	Long Term Evolution
MF	Matched Filter
NLMS	Normalized Least Mean Squares
OFDM	Orthogonal Frequency Division Multiplexing
PBR	Passive Bistatic Radar
PDCCH	Physical Downlink Control Channel
PSS	Primary Synchronization Signal
RCS	Radar Cross Section

RD	Range-Doppler
RF	Radio Frequency
RFI	Radio Frequency Interference
RLS	Recursive Least Squares
SAF	Self Ambiguity Function
SAR	Synthetic Aperture Radar
SC-FDM	Single-Carrier Frequency Division Multiplexing
SCR	Signal to Clutter Ratio
SINR	Signal to Interference and Noise Ratio
SNR	Signal to Noise Ratio
SSS	Secondary Synchronization Signal
TDD	Time Division Duplexing
UL	Uplink
URR	Unambiguous Radar Range
WSS	Wide Sense Stationary
WiMAX	Worldwide Interoperability for Microwave Access

List of Figures

List of Tables

DIRECT PATH INTERFERENCE SUPPRESSION AND RECEIVED SIGNAL PROCESSING FOR OFDM PASSIVE RADAR

I. INTRODUCTION

The basis of radar for detection of targets of interest is based on transmitting electromagnetic energy, receiving echoes from the transmitted signal and exploiting Electromagnetic (EM) properties for target detection, tracking and imaging. Passive radar takes advantage of the availability of non-cooperative emitters or emitters of opportunity such as commercial radio and television, other radars and mobile phone signals, and is by definition bistatic. A passive bistatic radar (PBR) system generally employs two receiving antennas; a reference antenna which collects the direct signal from the emitter and a surveillance which collects the echo signals from the targets of interest. In this thesis, reference will be made to a reference channel and a surveillance channel, corresponding to the signals received by the reference and surveillance antennas, respectively. The signal collected and stored in the reference channel is used to build a matched filter, which is applied to the surveillance signal and the output used to estimate target range and Doppler.

The aim of this thesis is to articulate Direct Path Interference (DPI) and explain how it poses a problem in passive radar. Methods that have been used to mitigate the problem will be detailed and analyzed for their applicability and effectiveness. The need for signal processing methods of DPI suppression will be shown, and different algorithms will be described, simulated and compared. OFDM signals will be analyzed as emitters of opportunity, specifically Long Term Evolution (LTE), DVB and Digital Audio Broadcasting (DAB) signals. Their structure will be described in order

to understand the implications in radar. Ambiguity functions for each signal will be shown, and methods to mitigate some of the signal features that are not desirable in a radar signal will be discussed. Exploitation of deterministic features of OFDM signals in processing the received signal will also be explored in this work. MATLAB® will be used to simulate scenarios to aid in the discussion throughout this thesis. The thesis will step through each of the parts of Figure 1 - defining the reference and surveillance signals, suppressing the DPI signal, processing the reference signal to remove or reduce the effects of OFDM signal structure, using the resulting signal to build a matched filter and processing the output of the matched filter to obtain a target range profile. Partially matched filters built from the deterministic features of OFDM signals will also be simulated and analyzed.

1.1 Thesis organization

Bistatic radar definitions are introduced in Chapter II, and DPI is defined and the problem it presents in passive radar is articulated. In chapter III, OFDM signals and their structures are described in order to understand their behaviour as radar signals. DPI suppression algorithms are discussed, analyzed and simulated in Chapter IV. Chapter V focuses on processing the reference signal to cancel the effects of some of the OFDM signal features that result in range ambiguities. Chapter VI gives the conclusion of the research and its potential extension into future work.

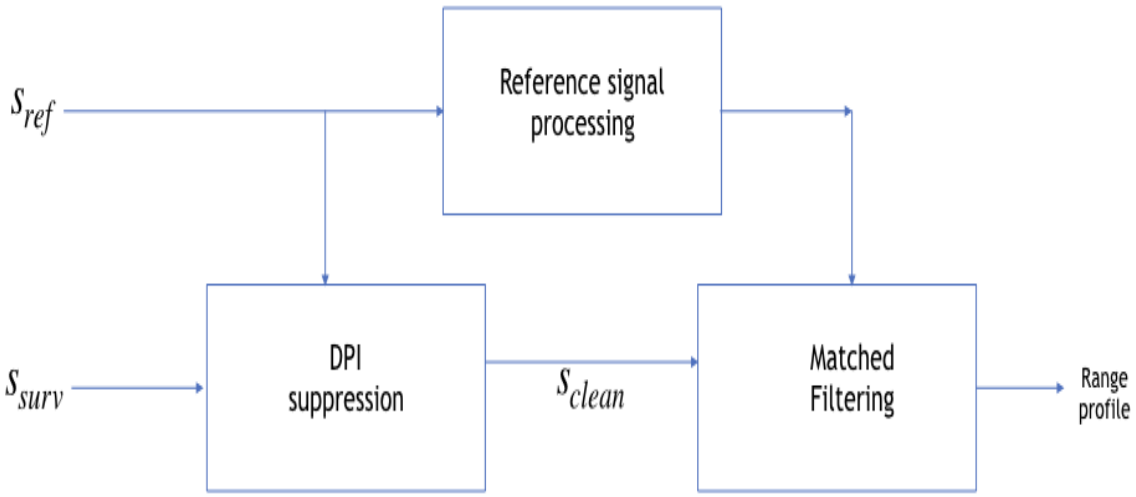

Figure 1. Passive radar signal processing

II. BISTATIC RADAR

The aim of this chapter is to define the parameters and describe the characteristics of bistatic radar, its merits and challenges, and extend the discussion to passive radar. The received and reference signals will also be defined and explained, and then extended to specific OFDM signals.

A bistatic radar is simply one operating with separated transmitting and receiving antennas; the receiver, transmitter and target are at different locations which can be on the ground or airborne and can be moving or stationary [4]. The advantages and disadvantages of PBR can be divided into two: those due to the bistatic geometry (advantages over monostatic radar) and those due to the system being passive (advantages over active radar). Bistatic radar can offer advantages over monostatic radar, but on the flip side comes with challenges not presented by monostatic radar. One advantage is angular diversity, which allows a target to be "viewed" from different angles, since Radar Cross Section (RCS) varies with β, which can enable detection of targets designed to be low-observable. On the other hand, the target can be located anywhere on a range contour and more signal processing and computation is required to determine the actual target location. The transmitted signal is also received directly at the receiver, resulting in interference that can lead to complete masking of weak target echoes. Passive radar then introduces further merits and challenges. Because the system does not transmit a signal, it can operate covertly. In addition, since existing signals are used, there is no requirement for the allocation of a specific operating frequency band, therefore passive radar is "green" in terms on bandwidth allocation. On the other hand, there is no control over the transmitted signal, therefore signal processing is made more challenging. Some of the challenges will be explored more in this work, particularly interference by the direct signal.

2.1 Geometry

A two-dimensional North-referenced coordinate system will be used to describe the bistatic geometry [4].

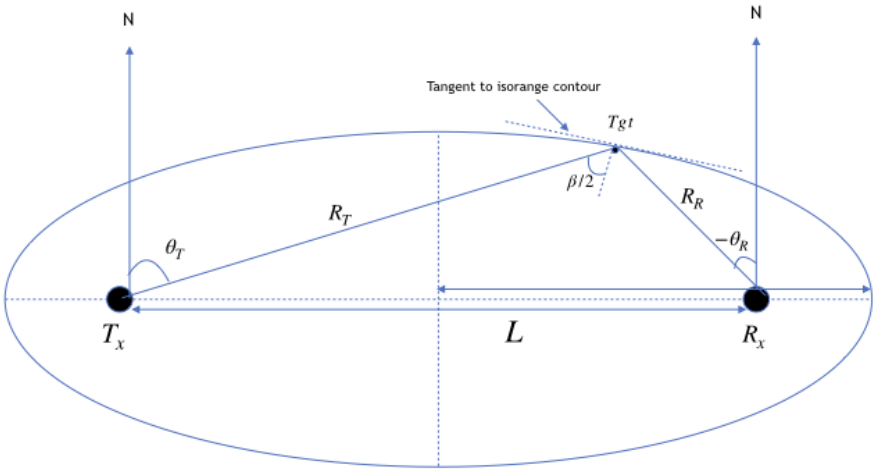

Figure 2. Basic bistatic radar geometry with North-referenced coordinate system

Figure 2 shows the basic bistatic geometry, where the transmitter, receiver and target can be anywhere in space and moving at any velocity. The plane containing the transmitter, receiver and target is know as the bistatic plane. R_T, R_R and L are the target range from the transmitter, target range from the the receiver and the distance between the transmitter and receiver respectively. L is referred to as the bistatic baseline. β is the angle between the transmitter and receiver with the vertex at the target [4]. θ_T and θ_R are known as the look angles and are measured clockwise from North [4]. From Figure 2, it can be seen that

$$\beta = \theta_T - \theta_R. \tag{1}$$

The bistatic range of the target is given by

$$R_b = R_T + R_R. \tag{2}$$

Any number of combinations of R_T and R_R can add up to the same bistatic range for a given bistatic baseline; therefore, the locus of an isorange contour describes an ellipse with the foci at the transmitter and receiver. The target can be located anywhere on the ellipse thus described, as long as it is such that it is illuminated by the transmitter.

2.2 Radar Range Equation

In a bistatic system, the power of the signal received is given by [5]

$$P_R = \frac{P_T G_T G_R \lambda^2 \sigma_B}{(4\pi)^3 R_T^2 R_R^2 L_T L_R} \tag{3}$$

where:

G_T is the transmitting antenna gain

G_R is the receiving antenna gain

σ_B is the bistatic Radar Cross Section (RCS) in square meters

L_T is the transmitting system losses, and

L_R is the receiving system losses

Thermal noise power at the receiver is given by

$$P_N = kT_0FB \tag{4}$$

where:

k is Boltzmann's constant

T_0 is the standard temperature (290 K)

B is the instantaneous receiver bandwidth in Hz, and

F is the noise figure of the receiver system (unitless)

The power of the echo signal from a target is scaled by the Radar Range Equation (RRE), and the relative powers of signals from targets being received at the same time by the same system depend on the targets' ranges and RCSs. In the simulations in this work, (3) was used to scale the power of received signals - it was important that the DPI was scaled such that its sidelobes masked real targets in order to show its effect and the effectiveness of DPI suppression.

2.3 Received Signal Model

To understand the DPI problem, it is important to understand what the signal received at the surveillance antenna looks like, that is, what it comprises and what form it takes. The signal received at the surveillance antenna is a superposition of target echoes, clutter echoes and the direct signal. Let s_{tx} be the transmitted signal and subscripts d, q, and i represent direct path, clutter, and target, respectively. Then, the received signal model is [3]

$$s_{surv}(t) = A_d(t)s_{tx}(t - L/c) + \sum_{q=1}^{Q} A_q(t)s_{tx}(t - \tau_q)e^{j2\pi f_{d,q}t}... \\ + \sum_{i=1}^{I} A_i s_{tx}(t - \tau_i)e^{j2\pi f_{d,i}t} + n(t) \tag{5}$$

where c is the speed of light, L is the bistatic baseline, and $A_{\{\cdot\}}$ represents the complex amplitude and phase terms associated with the direct path and echos. Furthermore, $\tau_{\{\cdot\}}$ and $f_{d,\{\cdot\}}$ denote the delay and Doppler terms, and $n(t)$ is noise. Even when signal-to-clutter ratio is large, direct path and echo relative timing must be well understood to process and interpret bistatic range profiles and images.

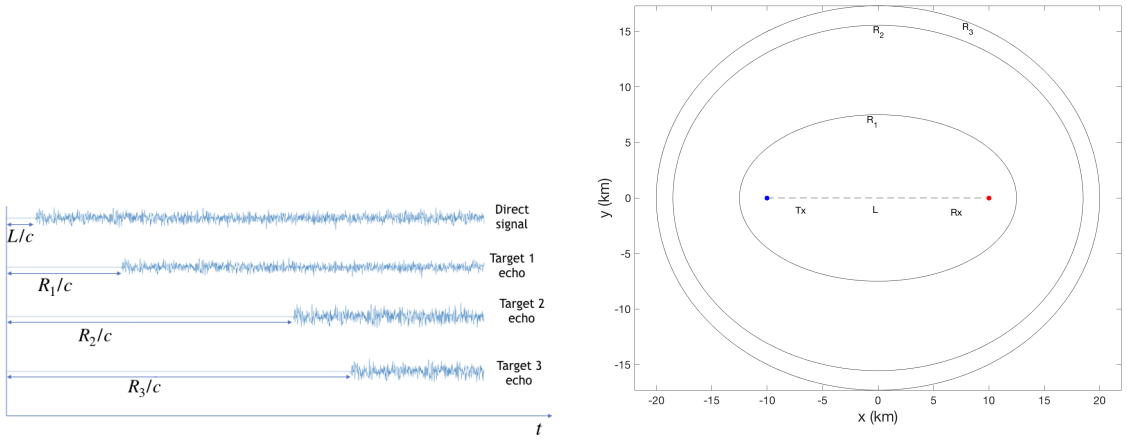

(a) Direct path and target signal timing

(b) Direct path and target range contours

Figure 3. Received signal relative timing and range contours

Figure 3(a) shows the relative delays of the transmitted signal as seen at the surveillance antenna, and Figure 3(b) shows the corresponding isorange contours. The signal seen at the surveillance antenna at any instant is a sum of all the signals present at that instant. The signals arrive at the surveillance antenna after a delay corresponding to the range of each target. Relating Figures 3(a) and 3(b), echoes from targets that lie at any bistatic range R will be received after a delay of R/c. The figures show three targets for simplicity of illustration, but in reality, there is a continuum of scatterer echoes arriving at the receiver, including returns from clutter. The signals cannot be separated in time or frequency, as will be discussed in Section 2.5, as well as the implications of this in terms of dealing with interference from clutter and the direct signal.

The clutter terms in (5) are discussed further in Section 4.1, which goes into details of how clutter and noise were modelled for simulation.

2.4 Reference signal model and matched filter

In order to build a matched filter, a portion of the direct signal from the transmitter to be captured by the reference antenna and processed. Ideally, the signal at the reference antenna would contain just the direct signal and white Gaussian system noise; however, copies of the signal due to multipath clutter are also received at the reference antenna. In addition, just as the direct signal leaks into the surveillance antenna, so can target echo signals leak into the reference antenna. It is therefore necessary to account for the presence of target echo signals in order to model a reference signal that approximates reality as closely as possible. The signal at the reference channel can therefore be expressed as

$$s_{ref}(t) = A_d(t)s_{tx}(t - L/c) + \sum_{q=1}^{Q} A_q(t)s_{tx}(t - \tau_q)e^{j2\pi f_{d,q}t}... \\ + \sum_{i=1}^{I} A_i s_{tx}(t - \tau_i)e^{j2\pi f_{d,i}t} + n(t), \tag{6}$$

although in this case, the clutter and noise terms would be different than those of the surveillance signal (a different realization of clutter and noise), but would be modelled similarly. The target echo amplitude and phase terms would also be different since the target returns would (ideally) couple into the reference antenna via lower gain sidelobes.

A matched filter is built from the signal in (6). The matched filter can be defined directly from this signal, since there is no way to separate the terms as they are superposed and they are copies of the same signal. The reference signal can also be processed further, as will be discussed in Subsection 3.2, to remove or suppress any features that would result in ambiguities in range or Doppler. The matched filter is defined such that the received signal is filtered to maximize Signal to Noise

Ratio (SNR) at a time delay corresponding to the target's range [5]. The matched filter that would maximize SNR for a reference waveform defined over the interval $0 \leq t \leq \tau$ is given by

$$h(t) = as^*_{ref}(-t) \qquad -\tau \leq t \leq 0 \tag{7}$$

and is a time-reversed complex conjugate form of the transmitted waveform; the arbitrary constant a is usually set to one [5]. If the reference signal is known, then the matched filter is known. Convolving the matched filter with the received waveform yields the matched filter output, designated $y(t)$, as

$$y(t) = \int_{-\infty}^{\infty} s_{surv}(\alpha)h(t-\alpha)d\alpha. \tag{8}$$

Substituting (7) into (8) results in

$$y(t) = a\int_{-\infty}^{\infty} s_{surv}(\alpha)s^*_{ref}(-(t-\alpha))d\alpha, \tag{9}$$

which is a correlation of the received signal with the reference signal, which is a captured copy of the transmitted signal. As discussed earlier in this section, the reference signal is unlikely to be a clean copy of the transmitted signal with additive system noise, but rather will contain clutter and possibly target echoes depending on the geometry and reference antenna orientation and pattern. Applying the definition of matched filter to the reference signal defined by (6) gives the impulse response of

the corresponding matched filter as

$$h(t) = A_d^*(-t)s_{tx}(-t + L/c) + \sum_{q=1}^{Q} A_q^*(-t)s_{tx}(-t + \tau_q)e^{-j2\pi f_{d,q}t}... \\ + \sum_{i=1}^{I} A_i^* s_{tx}(-t + \tau_i)e^{-j2\pi f_{d,i}t} + n(-t), \tag{10}$$

The effects of the presence of target echoes in the reference signal on the output of the matched filter will be explored in chapter IV.

2.5 Direct Path Interference

This section aims to articulate the problem of DPI by explaining how the direct signal causes interference and what effect it has, left unmitigated. In this thesis, the DPI signal is defined as the first term in (5). A PBR receiver consists of a reference antenna and a surveillance antenna; the reference antenna collects a signal directly from the transmitter from which to derive a Matched Filter (MF), while the surveillance antenna receives echo signals from which to estimate target ranges and Doppler. Ideally, both antennas are highly directional such that the reference antenna receives only the signal from the transmitter and the surveillance antenna receives only target echo signals. In reality, due to antenna radiation patterns, the signal received by the reference antenna includes not only the transmitted signal along a direct path, but also multipath copies of the signal as well as, potentially, target echo signals. The signal received by the surveillance antenna also includes a direct signal from the transmitter, which couples into the antenna via the main lobe or side lobes of the radiation pattern depending on the location and orientation of the surveillance antenna relative to the transmitter.

To understand the DPI problem, it is important to understand the signal described in (5); direct path and echo relative timing must be well understood to process and

interpret bistatic range profiles and images. The signal seen at the surveillance antenna at any instant is a sum of all the signals present at that instant. A comparison between pulsed and CW radar will be used to gain an understanding of the DPI problem and what solutions or mitigation strategies are feasible for CW radar, since the emitters of opportunity that will be explored in Section III (OFDM signals) are continuous signals. Consideration is given to two bistatic radar systems - a pulsed system and a CW system - in the same geometry and with the same two targets present. For simplicity of the illustration, the pulsed system transmits a simple pulse and the CW is a constant frequency cosine. Three pulses are shown for the pulsed radar system, and the CW radar signal is shown for the same amount of time as the duration of the three pulses for ease of comparison.

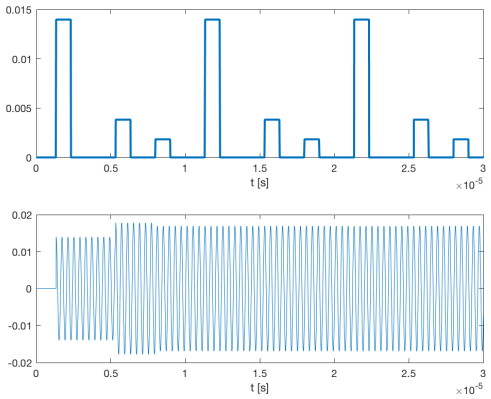

Figure 4. Received signals superposed - pulsed system and continuous system

Figure 4 shows the signal present at the receiver as described by (5). In the pulsed radar system it is possible to turn off the receiver for a duration of at least the bistatic baseline delay, thus preventing the direct signal being received. This approach is referred to as range gating, and is used in active pulsed radar to prevent the high power transmit signal from leaking into and damaging the receiver circuit [5]. Range gating divides the time between transmit pulses into multiple cells or range gates and results in elimination of excess receiver noise and clutter from competing with

the received signal [6]. Range gating works well for active pulsed radar, where the receiver is "blanked out" for the duration of the transmitted pulse plus an additional delay during which a return from the nearest target of interest is not expected, but a return from near field clutter could overload the receiver.

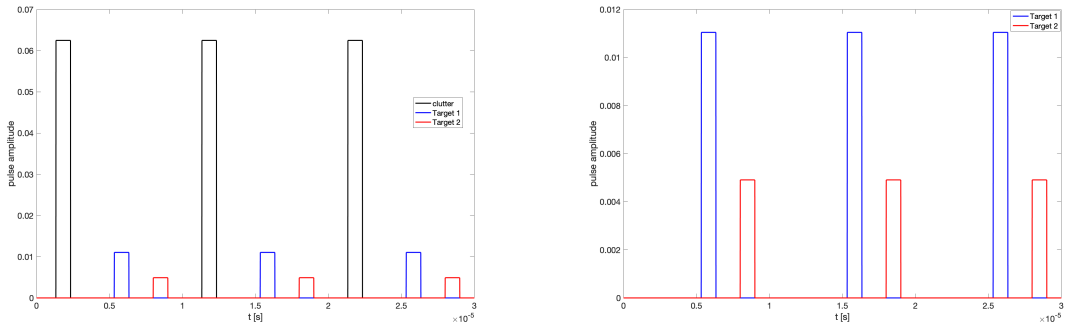

(a) Pulsed radar - no range gating

(b) Pulsed radar - after range gating

Figure 5. Pulsed radar - before and after range gating

A simplified example is considered, where there are two targets and one return from near range clutter. Figure 5(a) shows the transmitted pulses (top) and the received pulses (bottom), which include near range clutter. Figure 5(b) shows the received pulses with the receiver turned off for a period during which echoes from targets of interest are not expected, but near range clutter is.

2.6 DPI mitigation via range gating

In a bistatic pulsed radar system, range gating can be implemented to prevent the strong direct signal from coupling into the receive antenna and leaking into the receiver. Referring to Figures 3(a) and 3(b), since L is known, the receiver can be turned off for the corresponding delay, thereby using range gating to solve the DPI problem.

Range gating can be implemented in a pulsed monostatic and bistatic radar system

to prevent near range clutter and the direct signal from the transmitter from getting into the receiver based on the fact that each received echo from each scatterer is a pulse with a finite duration. In a CW radar system, however, the transmitted signal is present at all times, even when echo signals are being received.

It becomes clear that range gating can be implemented in a pulsed radar system by turning off the receiver for a sufficient time for every pulse, but a similar approach is not feasible in a continuous wave system because the direct signal is always present as long as the transmitter is transmitting a signal.

The level of DPI at the receiver depends on factors such as the bistatic baseline, receiver and transmitter antenna radiation patterns, coverage areas, and relative positions. The worst case scenario is when the bistatic baseline is small compared to target ranges, and the transmitter and receiver are in each other's antenna main lobes. DPI presents a more difficult challenge in CW radar than it does in pulsed radar. In a passive system, the problem is even more challenging because the user has no control on transmitter parameters and signal properties.

2.7 DPI Mitigation for CW bistatic radar

Having shown in the previous section that range gating to mitigate DPI is not feasible in CW radar since the direct signal and target echo signals cannot be separated in time, this section will describe mitigation strategies that have been shown to work and determine which methods provide the most utility in OFDM passive radar.

Mitigation of DPI can be accomplished in several ways - physical shielding, antenna null-steering and via signal processing algorithms. Physical shielding involves actually placing an EM shield to stop the direct signal from coupling into the reference antenna or placing the antenna and receiver such that the signal from the transmitter cannot reach the surveillance antenna. This method has been used suc-

cessfully in experimental works where the objective is to show viability of PBR using certain emitters of opportunity ([7], [8], [9]) as well as in systems where the transmitter and receiver are stationary. The disadvantage of physical suppression is that it limits the flexibility of the system and would not be practical for a moving (airborne) receiver as employed in Synthetic Aperture Radar (SAR) or for tracking moving targets. Adaptive antenna null-steering has also been demonstrated experimentally and via simulation; however, it is not flexible enough for a moving receiver.

DPI suppression in signal processing methods has been shown to be effective experimentally and via simulation. In [3] and [10], different DPI suppression algorithms were applied to experimental and simulated DVB data, and showed that they were effective.

2.8 Chapter conclusion

This chapter introduced definitions to be used throughout this work, defined DPI and presented the problem posed by DPI in CW passive radar.

III. OFDM PASSIVE RADAR

The OFDM waveforms of interest in radar are primarily designed for digital communications, and as such, their features are designed towards ensuring that the information sent can be decoded at the receiver - for example synchronization signals to identify the start of the useful information or convey information about the transmitter. Some features of OFDM signals may be desirable for radar applications (bandwidth), while others may not (synchronization features). To exploit OFDM communication signals as emitters of opportunity, it is important to understand the signals at the physical layer, that is, in the form in which they are physically transmitted on a channel. OFDM signal parameters are defined by standards, which are referred to in this thesis to define the signals and on which the MATLAB® simulated signals are based.

An OFDM signal is based on dividing an allocated bandwidth into subcarriers, each of which is modulated by the data to be transmitted. Synchronization and reference signals are then implemented. The inverse Fourier transform is taken to obtain the time-domain signal, to which a cyclic prefix is appended to the start of the symbol. A concatenation of symbols forms a frame; the number of symbols per frame is set by the signal standard. In the frequency domain, the allocated bandwidth is divided into individual subcarriers, separated in the frequency domain as specified by the signal standard.

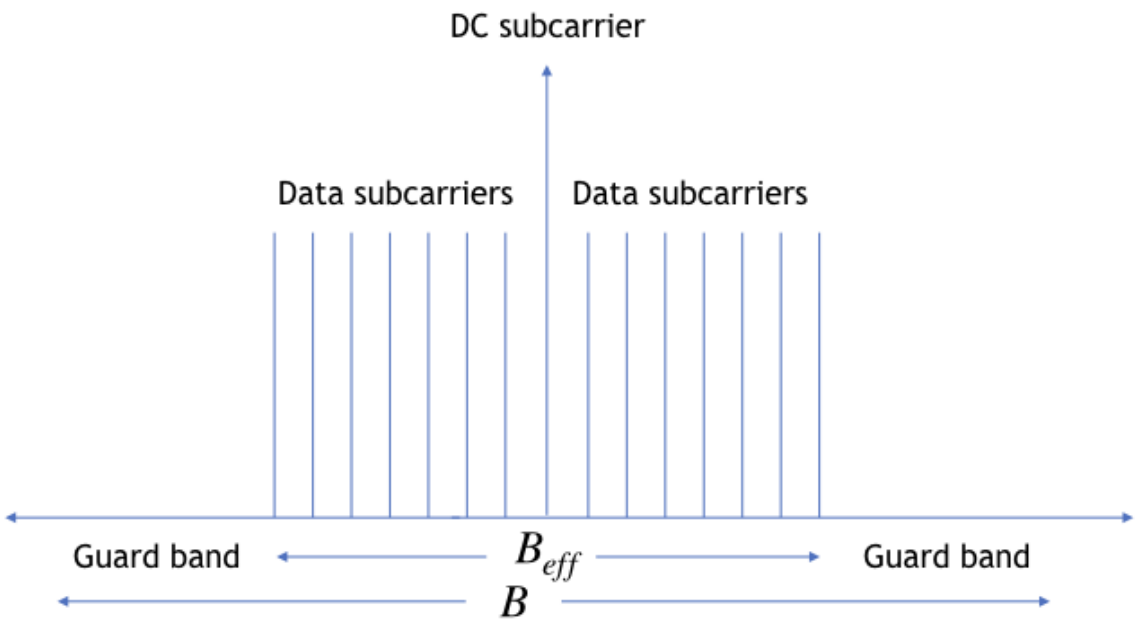

Figure 6. OFDM symbol spectrum[1]

The spectrum of one OFDM symbol is shown in Figure 6. The effective bandwidth spans the data-carrying subcarriers and DC subcarrier,

$$\Delta B = \Delta f(N_a)\Delta B_{eff} = \Delta f(N_a + 1) \tag{11}$$

where N_a is the total number of subcarriers, and N_a is the number of data-carrying subcarriers.

In the time domain, one symbol is the superposition of modulated subcarriers and is the inverse Fourier transform of the spectrum shown in Figure 6. The number of subcarriers per symbol is specified by the signal standard. Mathematically,

$$s(t) = e^{j2\pi f_0 t} \sum_{n=0}^{N-1} d_n e^{j2\pi n \Delta f t} \qquad -\tau \leq t \leq 0. \tag{12}$$

Figure 7 shows a few subcarriers, amplitude modulated by the data to be transmitted, and the sum of the subcarriers forming one OFDM symbol. A concatenation of

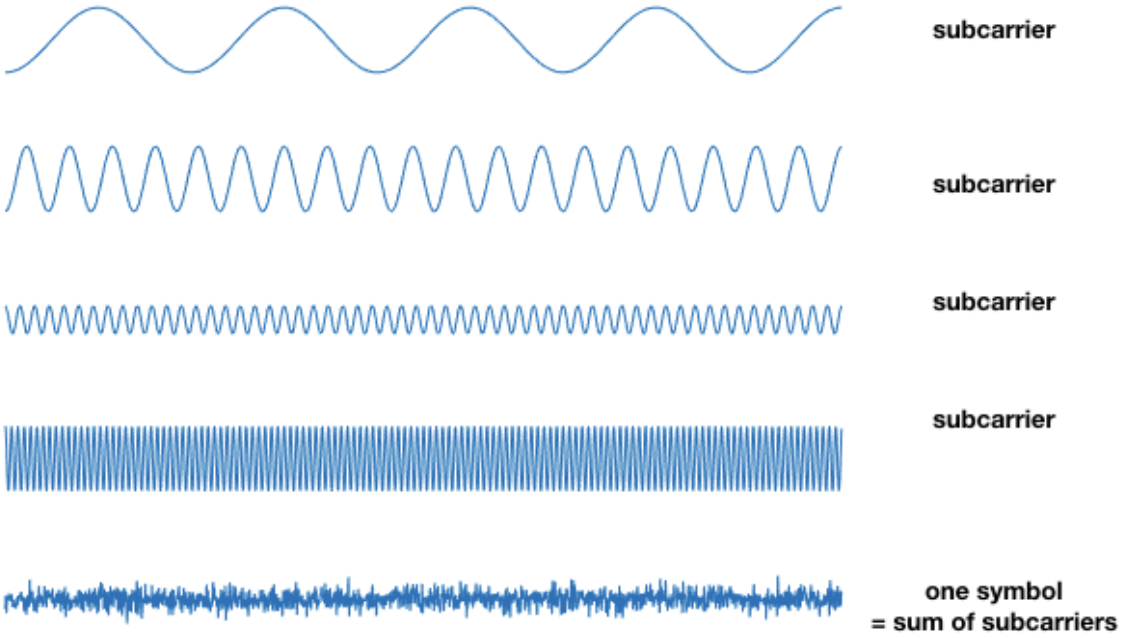

Figure 7. OFDM subcarriers and OFDM symbol

symbols forms a frame, the length of which is defined by the signal standard.

Such a signal could be applied as a radar signal and would behave as any other continuous signal [11]; however, OFDM signals include other features that need to be considered in applying them in passive radar. Their structure results in delay and Doppler ambiguities that need to be accounted for and mitigated for accurate range and Doppler estimation.

The Ambiguity Function (AF), used to characterize waveforms for radar application, is given by [12]

$$|x(\tau,\nu)|^2 = E\{|\frac{1}{E_s}\int_{-\infty}^{+\infty} s(t)s^*_{ref}(t+\tau)e^{j2\pi\nu t}dt|^2\}, \tag{13}$$

where $E\{.\}$ is the expectation operator over delay and Doppler, $s(t)$ and $s_{ref}(t)$ are the received and reference signals, τ and ν are the delay and Doppler between the

signals and $*$ denotes the complex conjugate. When $s(t) = s_{ref}(t)$, then the result is the Self Ambiguity Function (SAF), and it shows where peaks will occur in the range-Doppler profile due to the inherent signal structure. The ideal SAF has only one peak which occurs at zero delay and zero Doppler, referred to as a thumbtack AF (because it resembles an upside-down thumbtack). OFDM waveforms have been analyzed and characterized for passive radar applications via their AFs ([1], [12]), where the range and Doppler ambiguities due to signal structure were derived for LTE, DVB and DAB signals. The proceeding subsections discuss DPI and range ambiguities in the context of OFDM signals as emitters of opportunity for passive SAR; the AFs of LTE, DVB and DAB will be analyzed in Section 3.3. For the purposes of this thesis, a move-stop-move assumption is made for the receiver, such that the receiver is assumed stationary for the duration of receiving the signal to be processed as one pulse. Under this assumption, there is no receiver motion induced Doppler in the received signal, and therefore any Doppler ambiguities and non-zero Doppler range ambiguities are not relevant to the scope of this thesis and will not be discussed in depth.

The LTE standard consists of an Uplink (UL) and Downlink (DL) signal, which can be transmitted on the same frequency in different time slots (Time Division Duplexing (TDD)) or simultaneously in time on separate frequency bands (Frequency Division Duplexing (FDD)) [13]. FDD LTE presents a continuous signal for the purposes of passive radar. TDD LTE could be considered a pulsed signal and this can potentially be exploited to mitigate the effects of DPI through range gating.

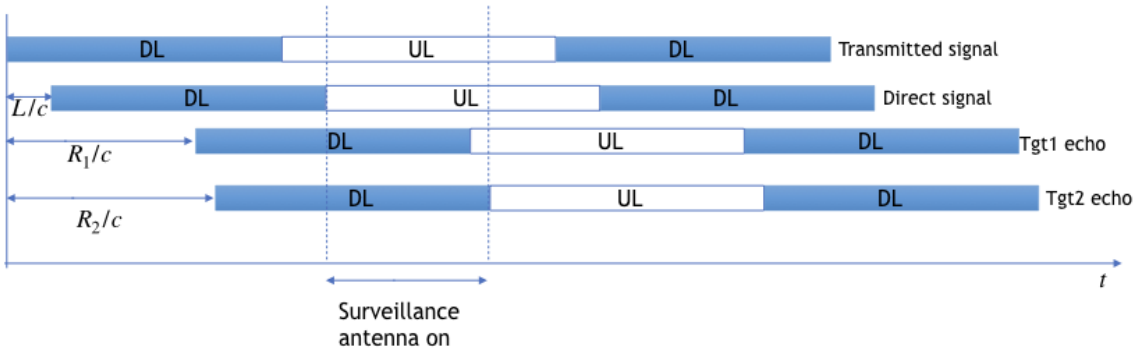

Figure 8. Signal relative timing example for TDD LTE

Figure 8 shows an example of the relative timing of the direct signal and the echoes from two targets, R_1 and R_2. Assuming that the passive radar system can be synchronized such that it is known when a DL frame ends, and the bistatic baseline L is known, then the surveillance antenna can be turned on at the time when it is expected that the direct signal being received will be the UL signal, while the target echoes of the DL frame are being received. The matched filter would be built from the DL frame; since the UL and DL frames contain different data, there cross-correlation would have no peaks and thus no response in the matched filter output due to the direct signal. TDD LTE was not considered any further as this work considered only FDD LTE with an extended Cyclic Prefix (CP).

3.1 OFDM signals as emitters of opportunity

OFDM signals have been shown experimentally and by simulation to be viable emitters of opportunity for passive radar. Experiments using OFDM signals for Moving Target Indication (MTI) have concluded that they are indeed viable emitters; the authors of [9] presented an AF analysis of an LTE FDD DL signal with an extended CP and experimental results from several moving target tracking scenarios. The AF analysis showed that range ambiguities were expected due to the CP at a delay of 66.67 μs either side of the main correlation peak, corresponding to a bistatic range

of 20 km; as this was outside the range of interest for the experiment, mitigating its effects was not presented. DPI was mitigated by physically placing the directional reference and surveillance antennas back-to-back such that the reference antenna faced the transmitter and the surveillance antenna faced the direction of the target. DAB signals were used in the experiment in [11] for MTI in a multistatic set up. The work was focused on addressing the challenge of interference by the direct signal and CP interference was not in its scope.

SAR imaging has also been shown to be possible using OFDM illuminators. In [7], the authors set up a small-scale experimental SAR imaging scene and used three types of OFDM waveforms: LTE, DVB and DAB as emitters of opportunity. Matched filtering and partially matched filtering were used to estimate the scene's phase history successfully. Worldwide Interoperability for Microwave Access (WiMAX) has also been shown to be a viable emitter of opportunity for passive SAR imaging; experimental results were presented in [14], which supported feasibility of OFDM-based SAR imaging. These works were aimed at exploring the feasibility of passive SAR imaging exploiting OFDM signals. The experiments were set up with a small bistatic angle with the transmitter and receiver co-located; highly directional antennas were used, which were faced towards the SAR scene, thus physically limiting how much of the direct signal coupled into the surveillance antenna. In addition, due to the small geometries involved, range ambiguities due to signal structure were not an issue in the scope of [7] and [14]. On a larger scale, passive SAR using DVB with an airborne receiver for ground imaging was presented in [15]. DPI mitigation was accomplished in two steps - the platform travelled between the illuminator and the imaged scene such that the reference and surveillance antennas could be placed on opposite sides of the platform, and the remaining direct signal was cancelled in processing via adaptive filtering. In [15] as well, range ambiguities were not within the scope and the

experimental set up was such that they did not present a source of interference.

3.2 DPI in OFDM passive radar

OFDM signals are continuous signals as far as their application to passive radar, therefore the discussion on DPI in CW radar readily extends to OFDM-based passive radar. The potential to consider OFDM frames or symbols as pulses and exploit their pulse-like frame and symbol structure to mitigate DPI is explored in Section is worth exploring.

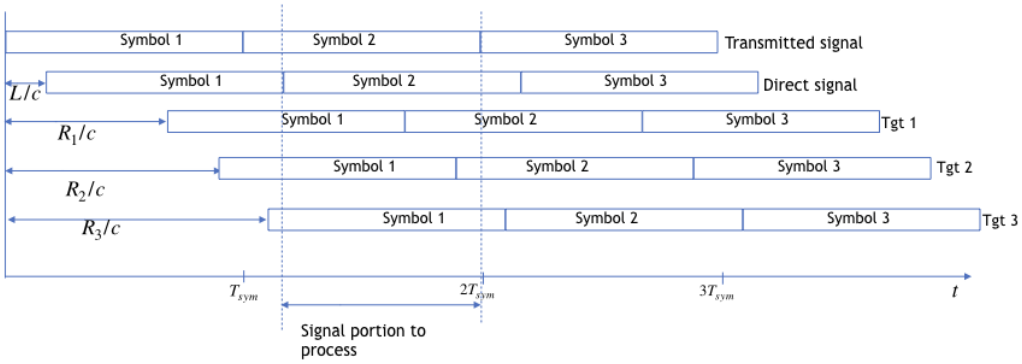

Figure 9. Relative timing for range gating

Figure 9 shows the relative timing of signals at the surveillance antenna for an example scenario.

Table 2. Example scenario ranges

L [km]	1.03
R_1 [km]	6.17
R_2 [km]	11.75
R_3 [km]	12.17

Table 2 shows the ranges of the targets. The portion of the signal processed is as shown in Figure 9, such that the direct signal does not contain symbol 1. A

matched filter is built from symbol 1, assuming that a direct signal has been perfectly captured by a reference antenna, which is applied to the surveillance signal portion and a range profile is retrieved from the matched filter output. Figure 11 shows the autocorrelation of an OFDM symbol (Figure 11(a)) and the cross-correlation between two adjacent symbols (Figure 11(b)) from the same frame containing user data. As expected, since the user data is unique from symbol to symbol, any two symbols will not correlate.

Substituting in the OFDM signal expression for s_{tx} in (5) yields

$$\begin{aligned} s_{surv} = A_d(t)e^{j2\pi f_0(t-L/c)} \sum_{n=0}^{N-1} d_n e^{j2\pi n\Delta f(t-L/c)} \ldots \\ + \sum_{q=1}^{Q} A_q(t)e^{j2\pi f_0(t-\tau_q)} \sum_{n=0}^{N-1} d_n e^{j2\pi n\Delta f(t-\tau_q)} \ldots \\ + \sum_{i=1}^{I} A_{tgt}e^{j2\pi f_0(t-\tau_i)} \sum_{n=0}^{N-1} d_n e^{j2\pi n\Delta f(t-\tau_i)} + \nu(t), \end{aligned} \tag{14}$$

where d_n is the complex amplitude of each subcarrier and $\nu(t)$ is additive white Gaussian noise (AWGN). What (14) means is that at any time at the surveillance antenna, the signal present is a superposition of target echo signals, the direct signal and AWGN. In addition, since the signal is continuous, there is no way of separating the direct signal from target echo signals as they are being received [11].

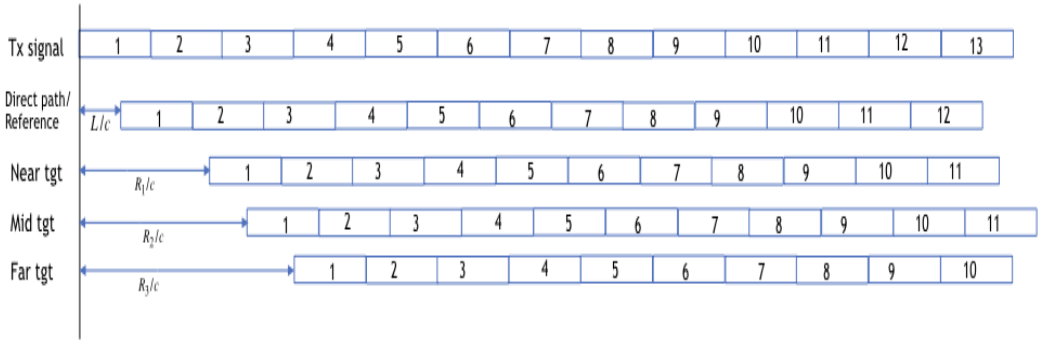

Figure 12. Received signal timing showing symbol numbers

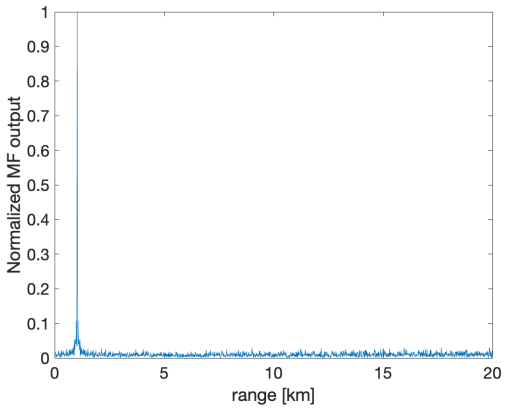

(a) No range gating, direct signal present

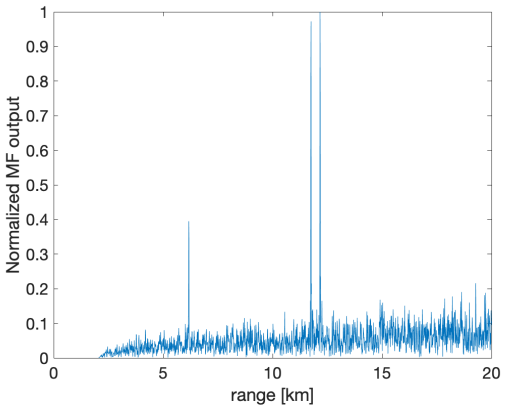

(b) No range gating, no direct signal present

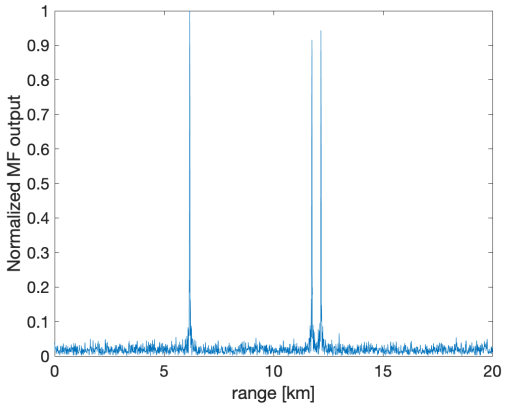

(c) Range gating, no direct signal present

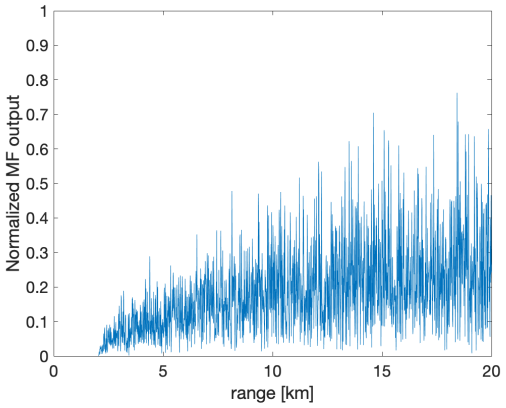

(d) Range gating, direct signal present

Figure 10. Range profiles showing results of range gating, with and without interference from a strong direct signal

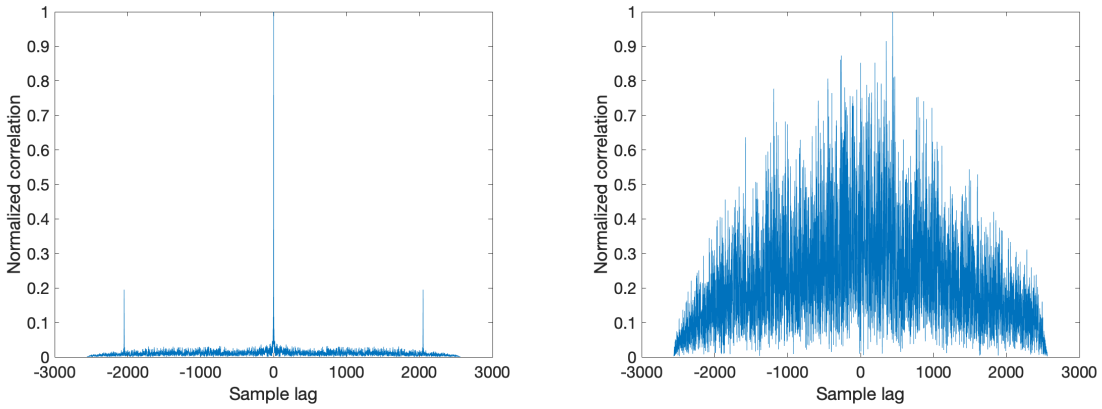

(a) Auto-correlation of one OFDM symbol

(b) Cross-correlation between two OFDM symbols from the same frame

Figure 11. Correlation of OFDM symbols

Figure 12 shows the relative timing of the transmitted signal and the signals received at the surveillance antenna, and shows the signals broken down into symbol numbers. Since the signals at the surveillance antenna are superposed, an OFDM signal behaves like any CW signal, and therefore, the discussion in Section 2.3 readily applies. The symbols or even frames can be treated as pulses, and range gating applied as discussed in Section III, since each symbol, and by extension each frame, of an OFDM signal contains different, uncorrelated, modulating data (user data). However, the received signal at any time still contains a strong direct path signal, which would dominate the matched filter output. The important difference between true pulsed radar and processing OFDM signals like pulsed radar is that with true pulsed radar, there is no signal transmitted between pulses; with an OFDM signal, however, even if each symbol is treated like a pulse, there is no point at which the transmitter stops transmitting between pulses or frames - at least not in any predictable pattern.

3.3 Effect of OFDM signal structure

The structure of OFDM signals introduces range and Doppler peaks in the AF other than at zero range and Doppler. These peaks mimic real targets and have to be taken into account and mitigated in order to fully utilize these signals in passive radar.

3.3.1 Cyclic prefix.

The CP is common to the OFDM signals considered in this thesis, and therefore the proceeding discussion applies to all, though LTE is used for illustration. The CP is an important part of OFDM signals and is implemented to prevent inter-symbol interference due to multipath propagation [16]. A CP is a copy of a portion of the signal taken from the end of the signal, that is appended to the start of the symbol, as shown in Figure 13. The CP is applied in the same way for LTE, DVB and DAB, the main difference being the proportion of the signal used for the CP, since the expected delay spreads due to multipath propagation differ among OFDM signals. Longer range signals are prone to longer delay spreads and therefore have longer CPs [16]. The impact of the CP in radar applications is due to the effect the CP has on the AF of signals to which a CP has been applied. The effect can then be extended to the output of a correlation matched filter and the resulting range-Doppler profile.

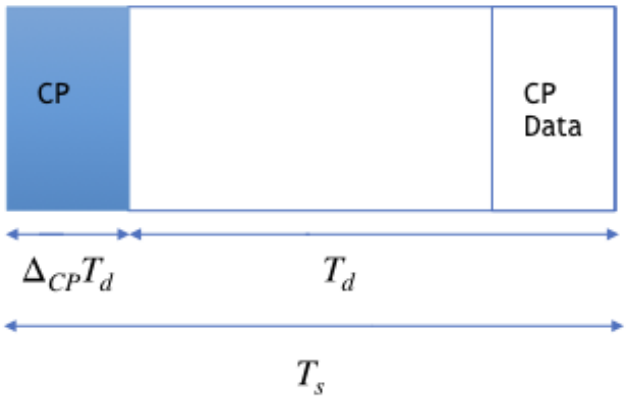

Figure 13. OFDM symbol in the time domain

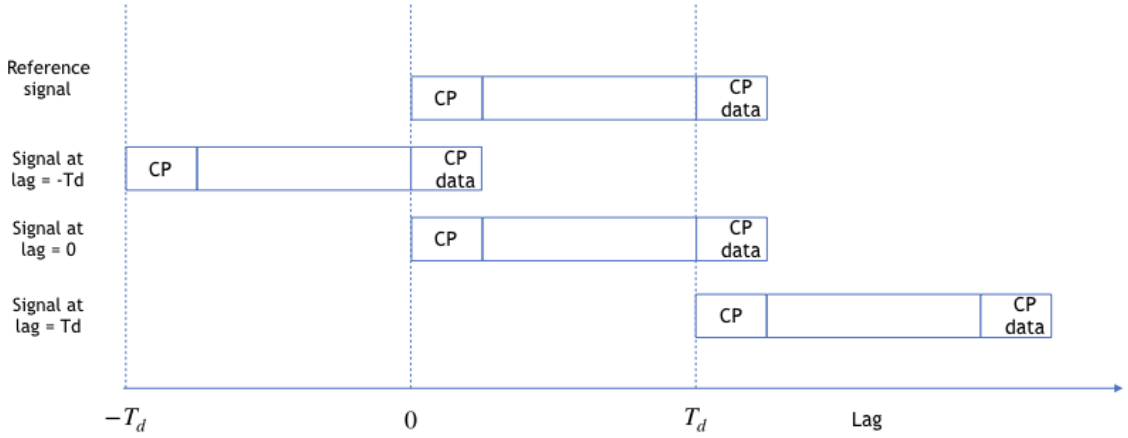

Figure 14. Effect of CP on autocorrelation

Figure 14 illustrates the effect of the CP on the output of a correlation MF. At a lag of $-T_d$, the CP lines up with the end of the symbol from which the CP data was taken, therefore, the leading CP peak occurs here. The same happens at a lag of T_d, and the trailing CP peak occurs. At zero lag, the entire symbol lines up and therefore the maximum correlation output occurs. The AF peak due to the CP, relative to the main peak, depends on Δ_{CP}, and is $20\log(\frac{T_{CP}}{T_{sym}})$ dB below the main peak, since the proportion of the signal that is correlated at a lag of $-T_d$ and T_d is $\frac{T_{CP}}{T_{sym}}$).

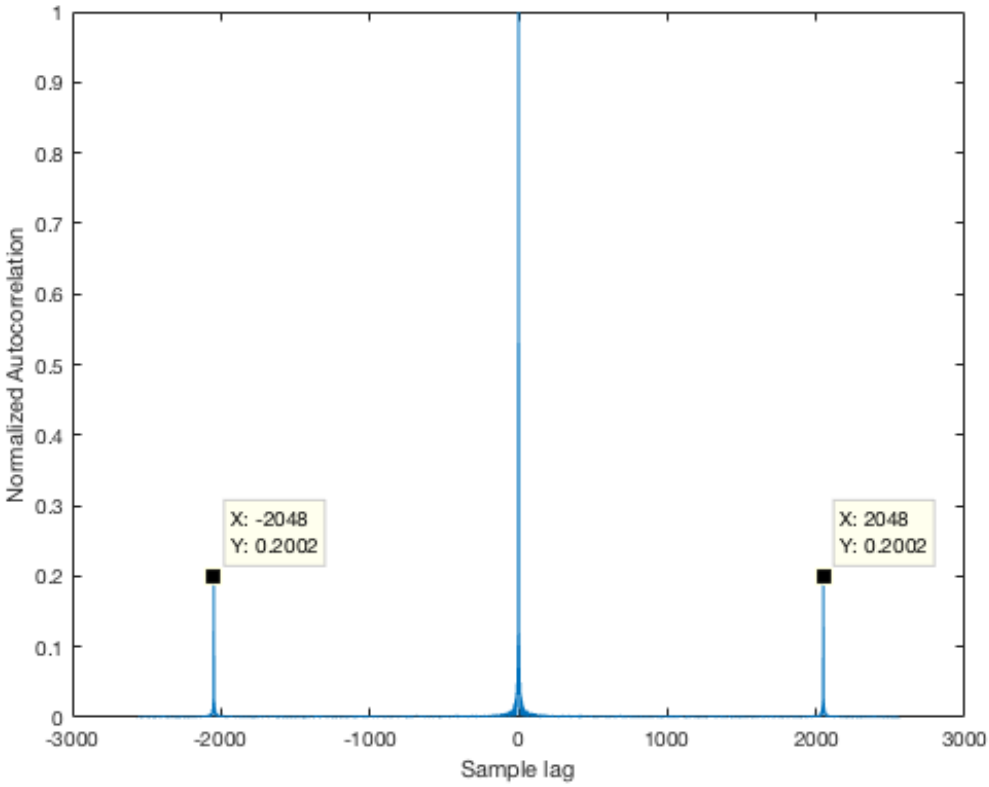

Figure 15. Autocorrelation of OFDM symbol with CP

Figure 15 shows the autocorrelation of one LTE symbol with $T_d = 2048$ samples and $\Delta_{CP} = 0.25$, over 1000 trials. Since an OFDM frame is a concatenation of symbols in the time domain, each of which has the same the autocorrelation of an entire frame will have the same peaks as those of a symbol.

The delay that the CP peak translates to depends on the signal parameters as defined in the signal's standard and can be computed as

$$\Delta t_{cp} = T_d t_s \tag{15}$$

where t_s is the sampling interval.

The length of the data part of the symbol, T_d, determines the unambiguous range

for OFDM signals with a CP; signals with a longer T_d will have a longer unambiguous range. The implications of the ambiguities resulting from the CP will depend on the signal, bistatic geometry, transmitter and receiver coverage areas and the application (imaging or MTI).

To understand where the CP peaks occur, a monostatic case is considered and the results extended to the bistatic case. For a monostatic system, range is given by

$$R = \frac{c\Delta t}{2} \tag{16}$$

where Δt is the round-trip delay time, i.e., the time between the signal being transmitted and an echo from the target being received. In the correlation MF output, the first CP peak (leading) occurs $T_d t_s$ seconds before the main (actual target peak); the second (trailing) CP peak occurs $T_d t_s$ seconds after the main peak. A delay of $T_d t_s$ seconds translates to a bistatic range of

$$R_{cp} = cT_d t_s. \tag{17}$$

The CP range therefore depends on the CP ratio relative to symbol length, which is different for different OFDM signals and is defined in the signals' standards.

The effect of the CP on range estimation is that the MF output for each target will have a peak at the target's true range and a CP peak either side of the main peak. The leading and trailing CP peaks will occur at ranges of $R - R_{cp}$ and $R + R_{cp}$ respectively.

In a bistatic system, as shown in Figure 2, the bistatic range of a target, $R_T + R_R$ is always less than the bistatic baseline, L due to the inherent properties of a triangle. The only exception is if a target lies on the bistatic baseline, but that case will not be considered in this paper, and any targets that lie directly between the transmitter

and receiver are not considered to be in the range of interest for the purposes of this work.

Table 3. Selected OFDM signal parameters

Signal	LTE	DVB	DAB
Data symbol duration (μs)	66.67	896	1000
CP ratio	1/4	1/4	63/256
CP range (km)	20	268.8	300
Bandwidth (MHz)	30.720	9.143	2.048
Effective bandwidth (MHz)	19.815	7.608	1.573
Range resolution (m)	7.56	19.70	95.29

Table 3 shows some signal parameters relevant to radar applications, including the CP range (bistatic) for LTE, DVB and DAB signals. The effect of the CP on target detection depends on the specific signal, the transmitter's illumination range and the ranges of the targets of interest.

3.3.2 LTE structure.

The LTE signal contains other deterministic features whose effects need to be understood and taken into consideration and even exploited in passive radar.

Primary and Secondary Synchronization signals.

Synchronization signals are used for detecting frame boundaries, cell search and handover [**?**]. This work considered FDD mode, in which the Secondary Synchronization Signal (SSS) and Primary Synchronization Signal (PSS) are placed in adjacent symbols in subframes 0 and 5. In the frequency domain, the synchronization signals occupy 72 subcarriers centered on DC.

Synchronization signals are transmitted at low power relative to user data, hence why the ambiguities do not show up in the SAF. They do , however, show up in the Cross Ambiguity Function (CAF) and therefore need to be taken into account and mitigated in order to get the correct range profiles from the output of a partially matched filter.

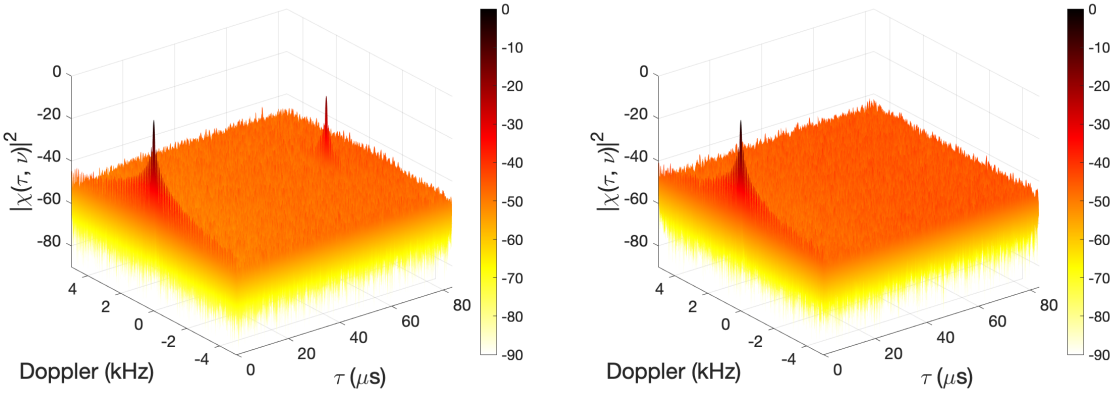

(a) LTE SAF

(b) LTE CAF with CP removed

Figure 16. LTE SAF and CAF

Figure 16 shows the SAF and CAF of one LTE frame; in 16(b), the reference signal has been processed to remove the peaks due to the CP as will be described in Chapter V.

Cell Specific Reference Elements.

Cell-Specific Reference Elements (CSRE)s are transmitted every DL frame, and are used for channel estimation and coherent demodulation. CSREs occur every 3 symbols, starting with the first symbol. Within each symbol that contains CSREs, they are spaced every 6 carriers; so in the frequency domain, every third subcarrier contains CSRE signals.

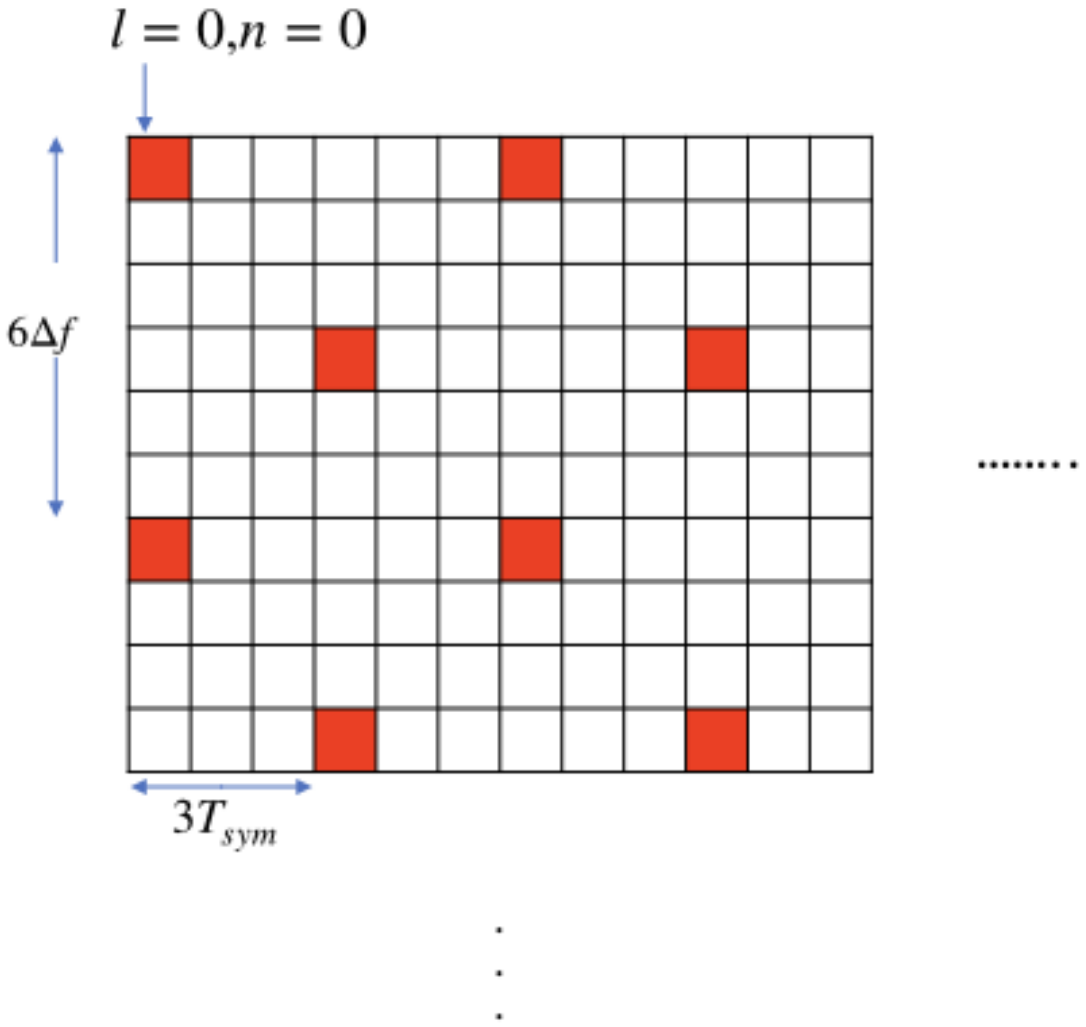

Figure 17. Locations of CSREs[1]

Figure 17 shows the location of the resource elements containing CSREs.

3.3.3 DVB structure.

The signal structure of the DVB signal introduces more range ambiguities than just the CP ambiguity. The 8k mode, which has 8192 carriers, will be considered in this work. A DVB frame is a concatenation of 68 symbols.

Table 4. DVB signal parameters

Data carrying sub-carriers	6817
Number of continual pilots	177
Number of scattered pilots	568
Number of TPS pilots	68
Carrier frequency	474 MHz
CP ratio	0.25
Effective bandwidth	7.6 MHz
Modulation	64-QAM

Table 4 shows the values specific to the DVB signal simulated using Air Force Institute of Technology (AFIT)'s Passive Radar Toolbox in MATLAB®.

Within each DVB frame, specified cells are modulated with known reference information used for synchronization, channel response estimation and transmission of system information [17]. There are three kinds of pilot signals inserted - continual pilots, scattered pilots and Transmission Parameter Signal (TPS).

In DVB 8k mode, there are 177 continual pilots, which are placed on all symbols at fixed subcarriers, as specified in the standard. The DVB continual pilot indices in the signal generated by the Passive Radar Toolbox is as specified in [17].

Scattered pilots occupy the same subcarriers every 4 symbols; within each symbol, they are placed every 12 subcarriers. The positions of the scattered pilots is given by

$$n_{SP} = n_{min} + 3(l \mod 4) + 12a \qquad a \in int, a \geq 0 \qquad n \in [n_{min} : n_{max}], \quad (18)$$

where l is the OFDM symbol index, n_{SP} is the subcarrier with the scattered pilots, $n_{min} = 0$ and $n_{max} = N$.

Scattered pilots result in ambiguities in delay, which can be shown by considering

the autocorrelation for one symbol of a signal containing only scattered pilots, s_{SP} [18]

$$\begin{aligned} R_{ss} &= \int_{-\infty}^{\infty} s_{SP}(t) s_{SP}^{*}(t+\tau) \\ &= \int_{-\infty}^{\infty} \sin(2\pi f_q t) \sin(2\pi f_q (t+\tau)) dt \\ &= \int_{-\infty}^{\infty} \sin(2\pi f_q t) \sin(2\pi f_q t + 2\pi f_q \tau) dt \end{aligned} \tag{19}$$

where

$$f_q = \frac{12}{T_U} q \quad q \in \text{int} \tag{20}$$

and T_U is the duration of the symbol excluding the cyclic prefix. Since in each symbol the sinusoids occur every 12 subcarriers. Peaks will occur in (19) for integer values of $f_q \tau$, which correspond to every $T_U/12$ s [18].

The scattered pilots occupy the same subcarriers every fourth symbol, therefore Doppler ambiguities occur every $1/4T_{sym}$. Due to the pattern with which the pilots occur, a continual and scattered pilot coincide every 4 symbols. Both continuous and scattered pilots are transmitted at a boosted power level of 16/9 of the power level of data subcarriers, and for this reason, peaks occur in the SAF of one symbol according to (19). Cancellation of peaks due to scattered pilots will be discussed in Chapter V.

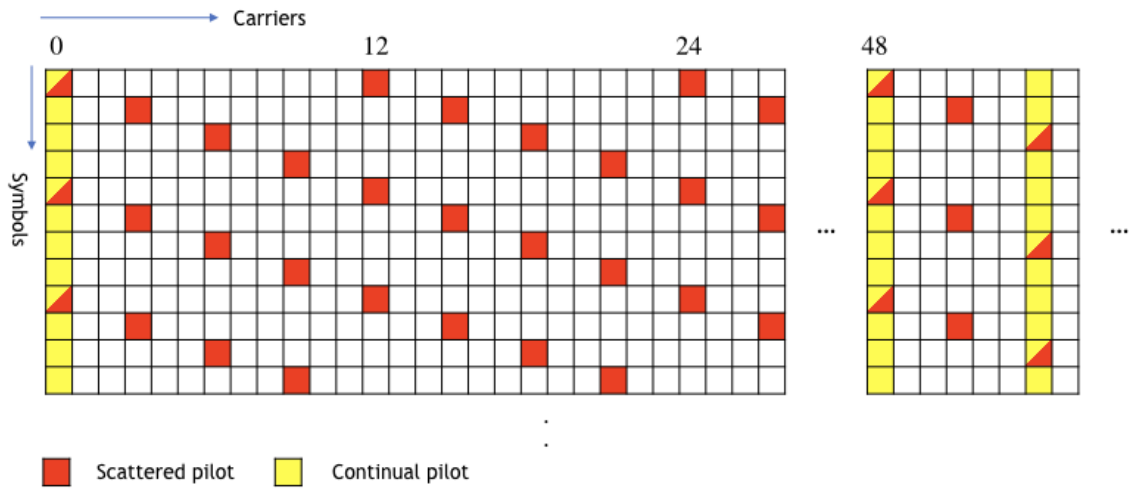

Figure 18. Location of scattered and continual pilots[2]

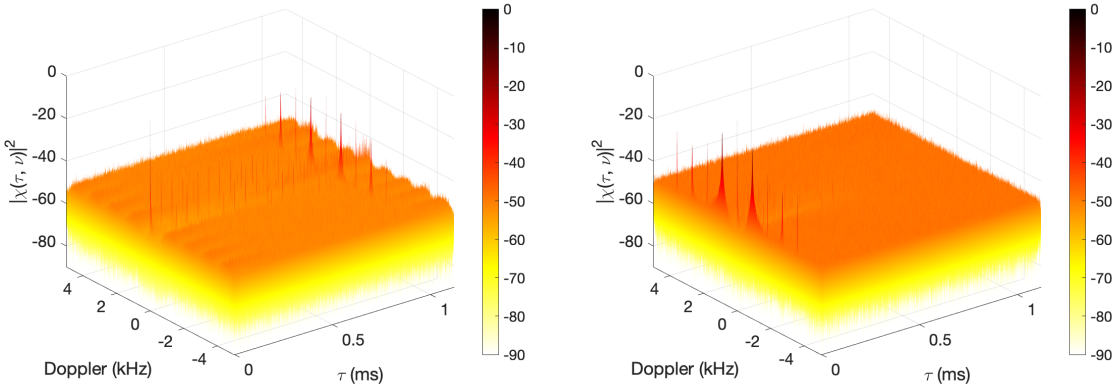

(a) SAF

(b) SAF with scattered pilots equalized

Figure 19. DVB SAF and improved SAF

3.3.4 DAB structure.

The DAB structure is simpler than the DVB structure; the synchronization channel is simply the first two symbols of the frame [19]. The first symbol is referred to as the null symbol, in which the transmitted signal is zero [19]. The second symbol provides the reference for the modulation of the proceeding symbol, which is the first data-carrying symbol of each frame. In the DAB signal, only the CP introduces range

ambiguity. On the other hand, the phase reference symbol is the only deterministic feature that can be used to build a partially matched filter.

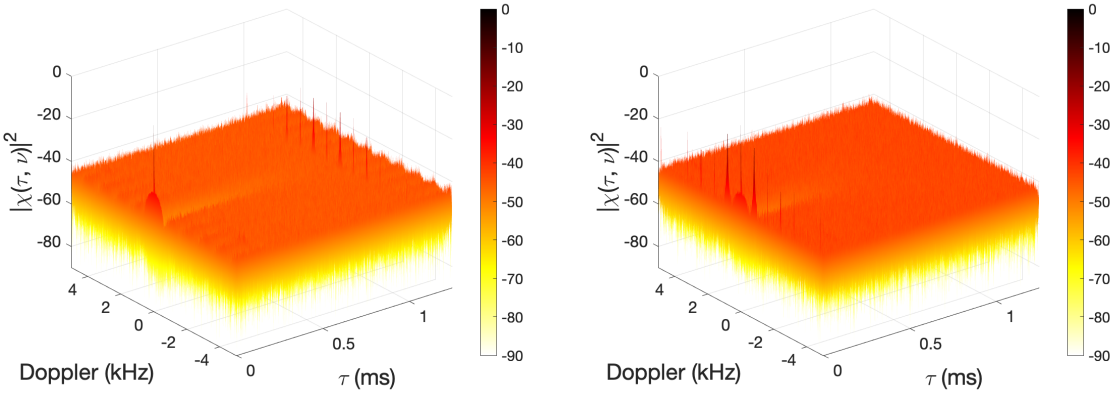

(a) SAF

(b) DAB CAF with CP removed

Figure 20. DAB SAF and CAF

Figure 20 shows the SAF of a DAB frame, and the CP peak can be seen at a delay of 1 ms in Figure 20(a), while in Figure 20(b), there are no CP peaks as the reference signal has been processed to zero the CP and CP data, which will be described in Chapter V.

3.4 Chapter conclusion

OFDM signal structures have been considered in the context of passive radar, and their effects on range-Doppler processing discussed. Their SAFs were also presented to provide a clearer understanding of the signals' behaviour when used in passive radar.

IV. RECEIVED SIGNAL PROCESSING

This chapter will cover processing the received signal to obtain the correct range profile. This will be done using a MATLAB® simulation; therefore, results and analysis will be included. Different DPI cancellation algorithms will be applied and compared/analyzed.

An example scenario will be used in this chapter to show the signal model and performance of the suppression algorithms and the resulting range profile after the application of each algorithm.

Table 5. Example scenario ranges

L [km]	5.01
R_1 [km]	11.75
R_2 [km]	15.51
R_3 [km]	18.67

Table 5 shows the bistatic baseline and ranges of three targets. For the example, a frame of each signal was processed as one pulse. Range profiles were generated for each signal type. The maximum range considered in the example was 20 km, which was picked to keep the example simple as there were no range ambiguities expected with any of the signals before 20 km (Chapter V will discuss range ambiguities and mitigation). In the scenario, the DPI signal power was set to approximately 30 dB above the average target signal power as given by

$$DPI[dB] = 10 \log \frac{P_{dpi}}{P_{tgts}}, \tag{21}$$

where P_{dpi} is the power of the direct signal. P_{tgts} is the average power of the target

echoes as given by

$$P_{tgts} = \frac{P_{total}}{N_{tgts}}, \tag{22}$$

where P_{total} is the total power of the target echo signal and N_{tgts} is the number of targets. In reality, each target return would have its own SNR, but for the purposes of the simulation, the average of the echo signal power was taken. The MF response of the target signals will be about 30 dB below the response of the direct signal, and, without suppression, will be masked by the response of the direct signal.

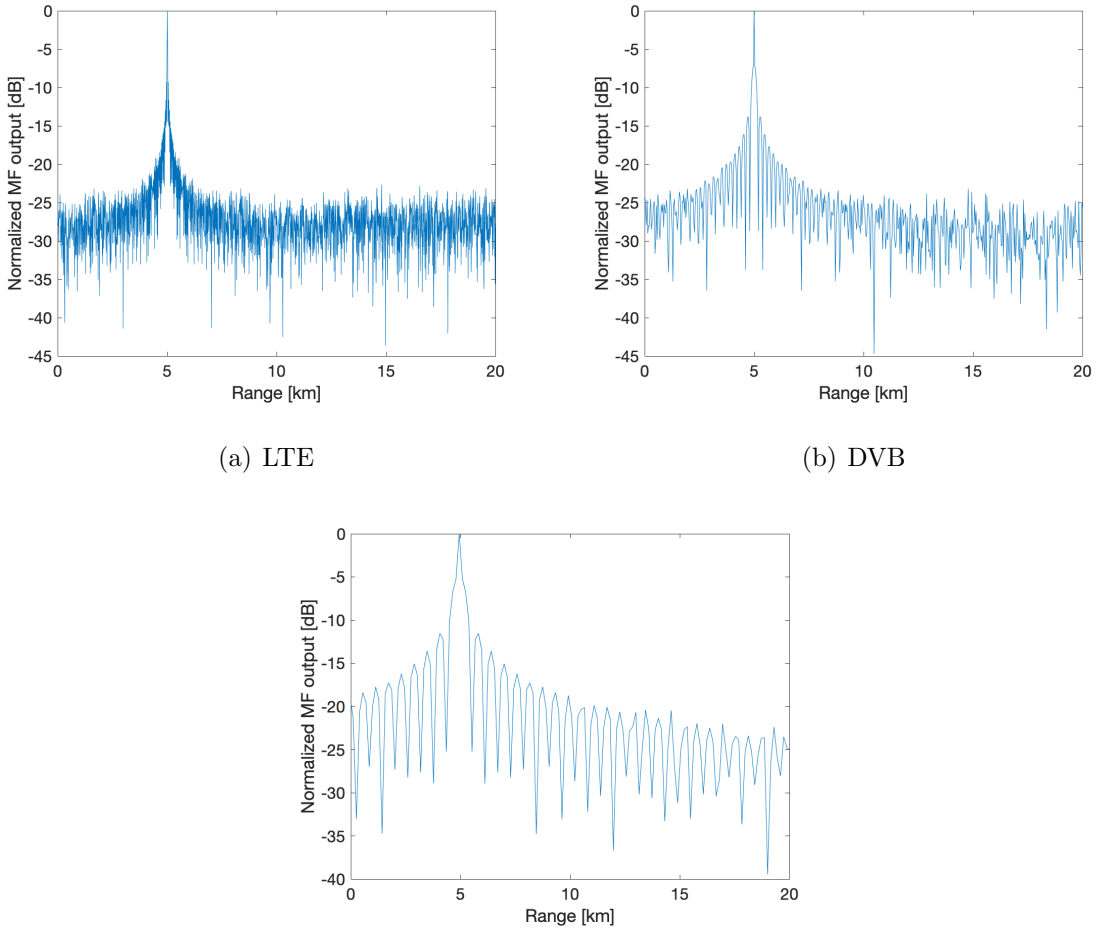

(a) LTE

(b) DVB

(c) DAB

Figure 21. Range profiles before DPI suppression

Figure 21 shows the resulting range profile in the presence of a strong direct signal with no DPI suppression applied.

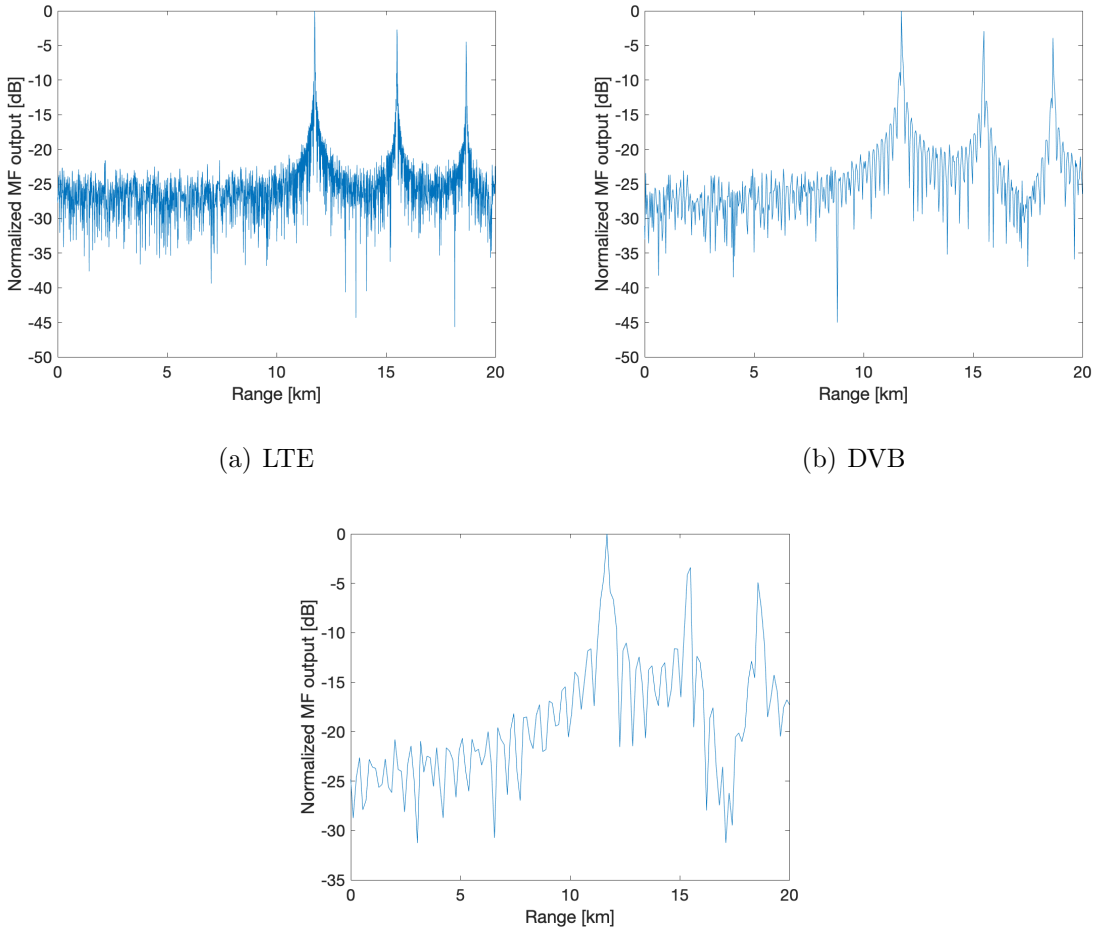

(a) LTE

(b) DVB

(c) DAB

Figure 22. Range profiles with no DPI present

Figure 22 shows what the range profiles would look like in the absence of DPI, and this provides a reference point for the desired range profiles after applying DPI suppression.

4.1 Noise and clutter Model

For the purposes of simulation, receiver system thermal noise was modelled as Gaussian random variables whose variance was computed from the desired SNR and the average target echo signal power such that

$$SNR = 10 * log(\frac{p_{tgt}}{p_n}), \tag{23}$$

where P_n is the receiver thermal noise power. SNR was varied by varying σ_{noise}.

Clutter was simulated as per the second term in (5),

$$s_{clut} = \sum_{q=1}^{Q} A_q(t) s_{tx}(t - \tau_q) e^{j2\pi f_{d,q} t}, \tag{24}$$

with one point scatterer per range bin, starting at the bistatic baseline and up to the maximum range of interest. The clutter complex amplitudes A_q were generated as Gaussian random variables whose variance was selected to achieve the desired Signal to Clutter Ratio (SCR), given by

$$SCR = 10 \log(\frac{p_{tgts}}{p_{clut}}), \tag{25}$$

where P_{clut} is the average power of the clutter signal. To generate the clutter complex amplitudes for a given SCR, the mean and standard deviation were scaled from the mean and standard deviation of the target complex amplitudes,

$$SCR_{lin} = 10^{0.1SCR} \tag{26}$$

$$\mu_{clut} = \frac{2\mu_{tgt}}{SCR_{lin}} \tag{27}$$

$$\sigma_{clut} = \frac{\sigma_{tgt}}{SCR_{lin}} \tag{28}$$

where μtgt and σ_{tgt} are the mean and standard deviation used to generate target complex amplitudes and $\mu clut$ and σ_{clut} are the mean and standard deviation for the clutter complex amplitudes.

One range bin was defined as being equal to the range resolution in width, and there was one clutter scatterer in the center of each range bin, except in those range bins with targets. The reasoning behind the clutter ranges is that the shortest clutter bistatic range will be greater than the bistatic baseline, and any targets beyond the maximum range will be processed out of the range profile. SCR was

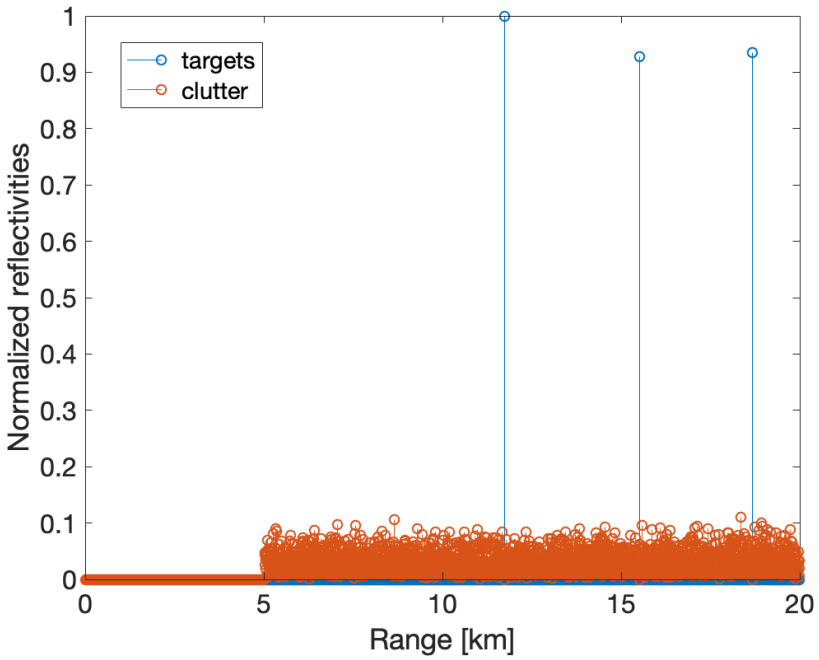

Figure 23. Relative reflectivities of targets and clutter

Figure 23 shows the relative reflectivities of clutter and target point scatterers, where the SCR is 40 dB. The clutter signal present at the reference and surveillance antennas was modelled by scaling the resulting clutter signal by the gains of the respective antennas in the direction of the targets, representing the worst case where all the clutter couples into the reference and surveillance antennas via their main lobes.

4.2 Matched Filter

The ideal matched filter is defined as the conjugate time reversed copy of the transmitted signal, and its impulse response at baseband is defined as (not considering Doppler)

$$h(t) = s^*(-t) \tag{29}$$

$$= \sum_{n=0}^{N-1} d_n^* e^{j2\pi n\Delta f t} \qquad -\tau \leq t \leq 0. \tag{30}$$

for one symbol.

Convolving the matched filter with the received signal is equivalent to a cross-correlation between the received signal and the reference signal. The matched filter thus defined requires that the transmitted signal be continuously captured and correlated with the received signal, the output of which is used to generate a range profile. As shown by (6), the signal received by the reference antenna is not necessarily a pure delayed copy of the transmitted signal, it may also contain some target echo signals as well as clutter returns, received via sidelobes. This model was used in order to approximate as closely as possible a real world reference signal. It was compared with an ideal reference signal with no clutter or target echoes in order to analyze what effect clutter and target echoes in the reference signal have.

An advantage of OFDM signals is that the signal properties and characteristics are defined in publicly available standards.The standards can be used to generate a signal that can be used to generate a partially matched filter.

4.3 DPI Cancellation algorithms

DPI suppression via signal processing methods allows for a strong direct signal present at the surveillance antenna. DPI suppression methods that have been pre-

sented in literature, and which provide a starting point for this research are

1. Wiener[20]
2. Extensive Cancellation Algorithm (ECA)[21]
3. Least Mean Squares (LMS)[20]
4. Normalized Least Mean Squares (NLMS)[20]
5. Fast Block Least Mean Squares (FBLMS)[20]
6. Recursive Least Squares (RLS)[20].

The DPI suppression algorithms listed work by estimating the DPI and subtracting it from the total signal present at the surveillance antenna, as shown in Figure 24. The Wiener, ECA and CLEAN are non-adaptive methods, while the last four above are adaptive algorithms.

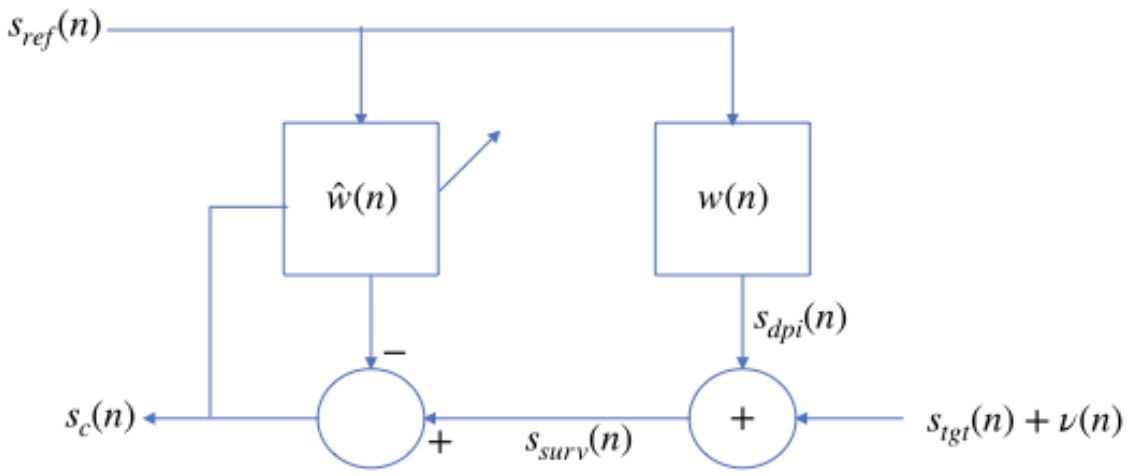

Figure 24. Adaptive filter block diagram [3]

The Wiener filter, LMS, NLMS, FBLMS and RLS algorithms are based on modelling the direct path as a filter as shown in Figure 24, whose coefficients are to be

estimated. The estimated filter is then convolved with the reference signal, resulting in an estimated DPI signal, which is subtracted from the surveillance signal. The resulting signal is then applied to a matched filter and the output processed to produce a range profile. In this thesis, to quantify the DPI suppression achieved, first, Signal to Interference and Noise Ratio (SINR) was defined as

$$SINR = 10\log(\frac{P_{tgt}}{P_n + P_{clut} + P_{dpi}})$$

where P_{dpi} is the power of the direct signal. Suppression was then defined as

$$suppression[dB] = SINR_S - SINR_{NS}, \tag{31}$$

where $SINR_{NS}$ and $SINR_S$ are the values of SINR before and after suppression.

4.3.1 Wiener Filter.

To derive the Wiener filter, the estimate of the direct signal present at the receiver was defined as $s_{d(est)} = \sum_{m=0}^{M-1} \hat{w}(m)s_{ref}(n-m)$, where $\hat{w}$ models the direct and multiple paths through which the direct signal passes before reaching the surveillance

antenna. The Mean Squared Error (MSE) is then defined as

$$
\begin{aligned}
E[e^2(n)] =& E[(s_{dpi}(n) - s_{d(est)}(n))^2] && (32)\\
=& E[(s^2_{dpi}(n) - 2(s_{dpi}(n)s_{d(est)}(n) + s^2_{d(est)}(n)] && (33)\\
=& E[s^2_{dpi}(n)] - 2E[(s_{dpi}(n)s_{d(est)}(n)] + E[s^2_{d(est)}(n)] && (34)\\
=& E\left[\sum_{k=0}^{M-1}\sum_{m=0}^{M-1}\hat{w}(k)\hat{w}(m)s_{dpi}(n-k)S_d(n-m)\right] && (35)\\
& - 2E\left[\sum_{m=0}^{M-1}\hat{w}(m)s_{dpi}(n-m)s_{ref}(n)\right] - R_d(0)\\
=& \sum_{k=0}^{M-1}\sum_{m=0}^{M-1}\hat{w}(k)\hat{w}(m)R_d(k-m) && (36)\\
& - 2\sum_{m=0}^{M-1}\hat{w}(m)R_{rd}(m) - R_d(0).
\end{aligned}
$$

where s_{dpi} is the direct path interference signal that is to be estimated, R_{rd} is the cross-correlation between the reference signal and direct signal and R_d is the autocorrelation of the direct signal. In matrix notation,

$$
E[e^2(n)] = \underline{\hat{\mathbf{w}}}^T\underline{\underline{\mathbf{R}}}_{\mathbf{r}}\underline{\hat{\mathbf{w}}} - 2\underline{\hat{\mathbf{w}}}^T\underline{\mathbf{R}}_{\mathbf{rd}} - R_d(0), \tag{37}
$$

where

$$
\underline{\hat{\mathbf{w}}} = \begin{bmatrix} \hat{w}(0) \\ \hat{w}(1) \\ \vdots \\ \hat{w}(M-1) \end{bmatrix}, \tag{38}
$$

$$\underline{\mathbf{R}}_{\mathbf{rd}} = \begin{bmatrix} R_{rd}(0) \\ R_{rd}(1) \\ \vdots \\ R_{rd}(M-1) \end{bmatrix} \tag{39}$$

and

$$\underline{\underline{\mathbf{R}}}_{\mathbf{r}} = \begin{bmatrix} R_r(0) & R_r(1) & \cdots & R_r(M-1) \\ R_r^*(1) & R_r(0) & \cdots & R_r(M-2) \\ \vdots & \vdots & \ddots & \vdots \\ R_r^*(M-1) & R_r^*(M-2) & \cdots & R_r(0) \end{bmatrix}_{MxM}, \tag{40}$$

noting that $\underline{\hat{\mathbf{w}}}$ is defined to be causal and therefore an FIR filter. FIR filters are preferable both in theory and in practice because they are stable which is desirable when a filter is required to be adaptive as it avoids the added complexity of inherently unstable IIR filters in an already complex problem [20]. Finding the gradient of the MSE and equating it to zero,

$$\nabla_{\mathbf{w_{est}}} J = \nabla_{\underline{\hat{\mathbf{w}}}}(\underline{\hat{\mathbf{w}}}^T \underline{\underline{\mathbf{R}}}_{\mathbf{r}} \underline{\hat{\mathbf{w}}} - 2\underline{\hat{\mathbf{w}}}^{\mathbf{T}} \underline{\mathbf{R}}_{\mathbf{rd}} - R_d(0)) \tag{41}$$

$$= \nabla_{\underline{\hat{\mathbf{w}}}}(\underline{\hat{\mathbf{w}}}^T \underline{\underline{\mathbf{R}}}_{\mathbf{r}} \underline{\hat{\mathbf{w}}}) - \nabla_{\underline{\hat{\mathbf{w}}}}(2\underline{\hat{\mathbf{w}}}^{\mathbf{T}} \underline{\mathbf{R}}_{\mathbf{rd}}) - \nabla_{\underline{\hat{\mathbf{w}}}}(R_d(0)) \tag{42}$$

$$= 2\underline{\underline{\mathbf{R}}}_{\mathbf{r}} \underline{\hat{\mathbf{w}}} - 2\underline{\mathbf{R}}_{\mathbf{rd}} - 0 \tag{43}$$

the optimal filter $\underline{\hat{\mathbf{w}}_*}$ can be solved for as

$$2\underline{\underline{\mathbf{R}}}_{\mathbf{r}}\underline{\hat{\mathbf{w}}_*} - 2\underline{\mathbf{R}}_{\mathbf{rd}} = 0 \tag{44}$$

$$\underline{\underline{\mathbf{R}}}_{\mathbf{r}}\underline{\hat{\mathbf{w}}_*} = \underline{\mathbf{R}}_{\mathbf{rd}} \tag{45}$$

$$\underline{\hat{\mathbf{w}}_*} = \underline{\underline{\mathbf{R}}}_{\mathbf{r}}^{-\mathbf{1}}\underline{\mathbf{R}}_{\mathbf{rd}}. \tag{46}$$

The estimated filter is then convolved with the reference signal to obtain an estimate of the DPI signal.

The variable parameter for the Wiener filter is the filter length; too few tap weights means that the estimated filter will be shorter than the actual system response and therefore the estimated DPI signal will be farther from the actual signal. A longer filter results in the remainder of the estimated tap weights being close to zero and therefore has an effect only run time and not a significant enough effect on the resulting DPI estimate. In addition, a longer filter length increases the algorithm's run time by increasing the size of the reference signal correlation vector and surveillance signal correlation matrix, whose sizes are $M \times 1$ and $M \times M$ respectively. It was therefore important to find a filter length that resulted in sufficient suppression with as short a run time as possible.

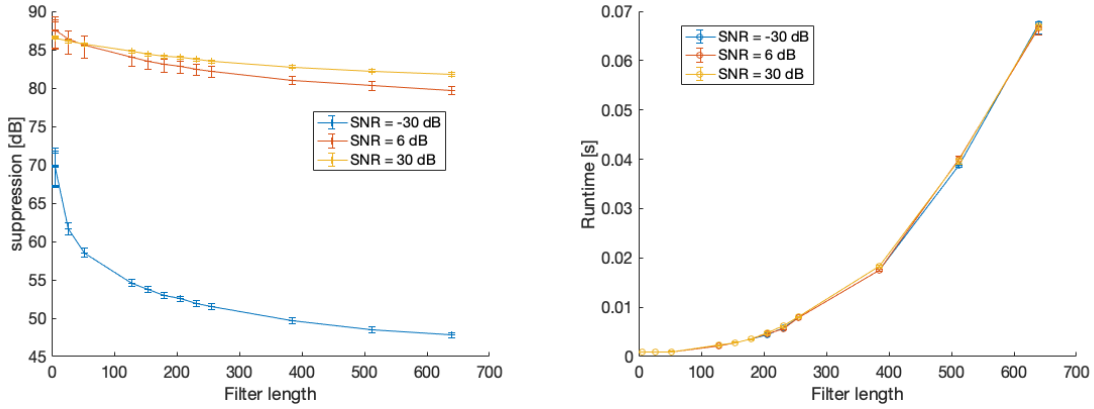

(a) suppression versus filter length

(b) suppression versus runtime

Figure 25. Wiener: Effect of filter length on suppression and runtime, signal length = 2560

Figure 25 shows suppression and runtime for varying filter lengths at a high, moderate and low SNR, averaged over 500 trials. The run time increased approximately exponentially with filter length, with the suppression values remaining within 10 dB for higher SNRs and 20 dB for an SNR of -30 dB. A filter length of 0.01% of the surveillance signal length was found to result in sufficient suppression for different signal lengths, while keeping run time low as compared to a longer filter length. Sufficient suppression in the case of the scenario used is defined as at least 30 dB, such that the MF response of the targets was at least equal to the response due to DPI. The minimum filter length was set to 5 when 0.01% of the signal length was less than 5.

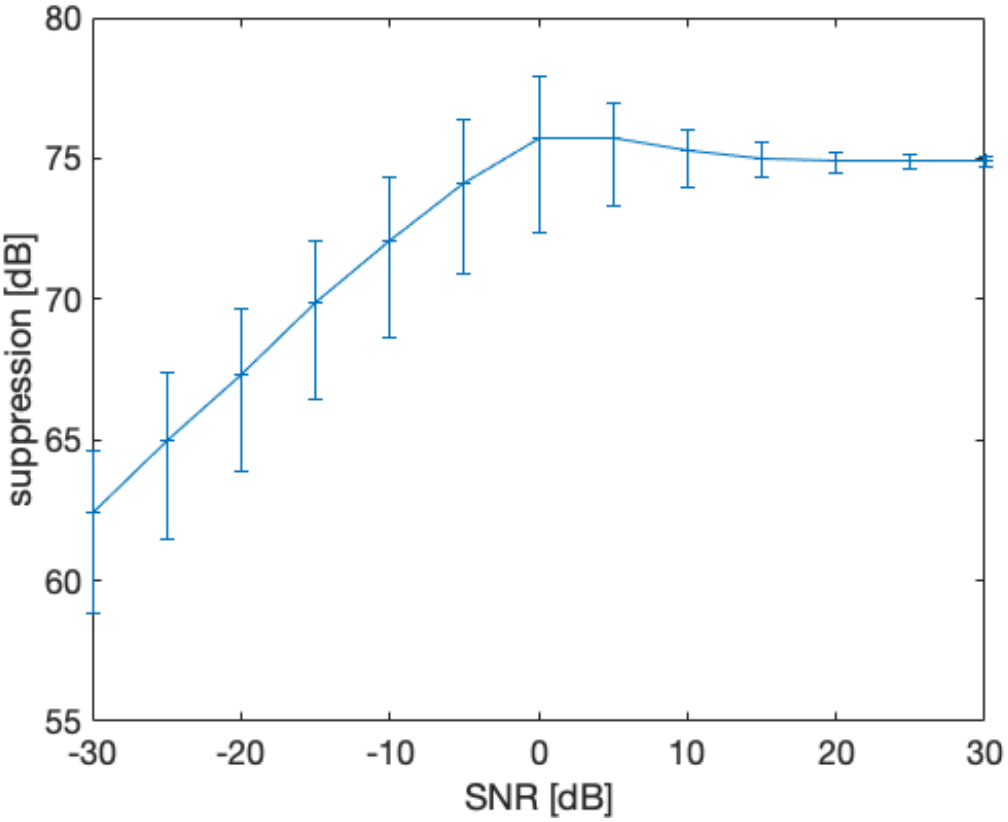

Figure 26. Wiener filter performance with varying SNR

The performance of the Wiener filter is shown in Figure 26 over 1000 trials, with error bars at the 25^{th} and 75^{th} percentiles. At a low SNR, suppression decreases by less than 15 dB from the suppression at the highest SNR tested, with a deviation of 2.5 dB either side of the mean; the deviation does not vary significantly below an SNR of 0 dB, which means that the Wiener filter maintains its performance with decreasing SNR, at least to the minimum SNR tested.

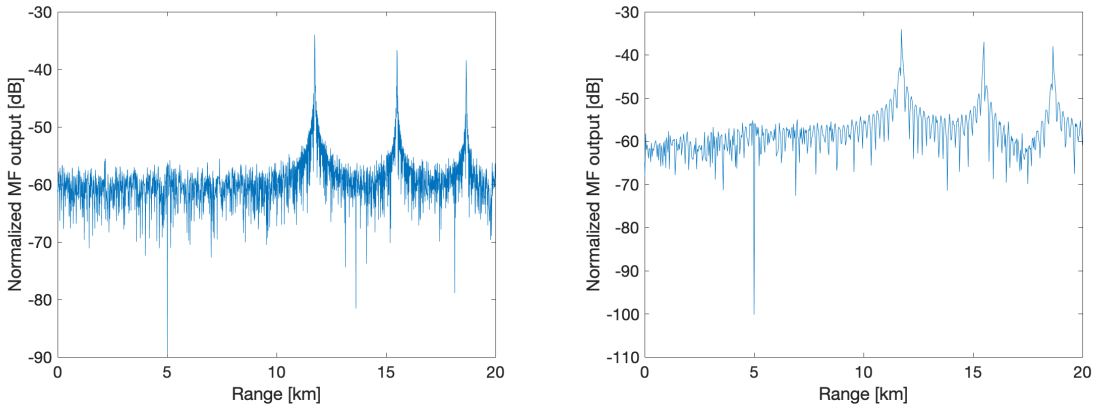

(a) LTE

(b) DVB

(c)

DAB

Figure 27. Range profiles after applying Wiener filter

Figure 27 shows the range profiles after applying the Wiener filter for DPI suppression. The MF output is normalized to the maximum response prior to suppression such that the response due to DPI before suppression is at 0 dB. The target responses that were more than 30 dB below the direct signal are now visible.

4.3.2 Extensive Cancellation Algorithm.

ECA was proposed in [22], and is based on projecting the received signal in a subspace that is orthogonal both to the interfering signal and previously detected targets. The estimated filter tap weights is given by

$$\underline{\hat{\mathbf{w}}}_{ECA} = (\underline{\underline{\mathbf{X}}}^H \underline{\underline{\mathbf{X}}})^{-1} \underline{\underline{\mathbf{X}}}^H \underline{\mathbf{s}}_{surv} \tag{47}$$

where $\underline{\underline{\mathbf{X}}}$ is a matrix of delayed, Doppler-shifted replicas of the reference signal [23, 24],

$$\underline{\underline{\mathbf{X}}} = \begin{bmatrix} \underline{\mathbf{s}}_{ref}(t-0) \\ \underline{\mathbf{s}}_{ref}(t-\tau_1) \\ \underline{\mathbf{s}}_{ref}(t-\tau_2) \\ \vdots \\ \underline{\mathbf{s}}_{\mathbf{ref}}(t-\tau_M) \end{bmatrix} \tag{48}$$

and M is the number of delay bins, with the reference signal delayed by a duration τ from 0 to a specified maximum. The estimated DPI signal is a convolution of the estimated filter and the reference signal. Only one Doppler bin was used (zero Doppler) in the simulation as there were no Doppler shifted target or clutter echoes to be accounted for.

For ECA, the variable parameters are the number of range and Doppler bins. For this work only one Doppler bin (zero Doppler) was used for simulation. The number of delay bins was varied and the DPI suppression computed for each case.

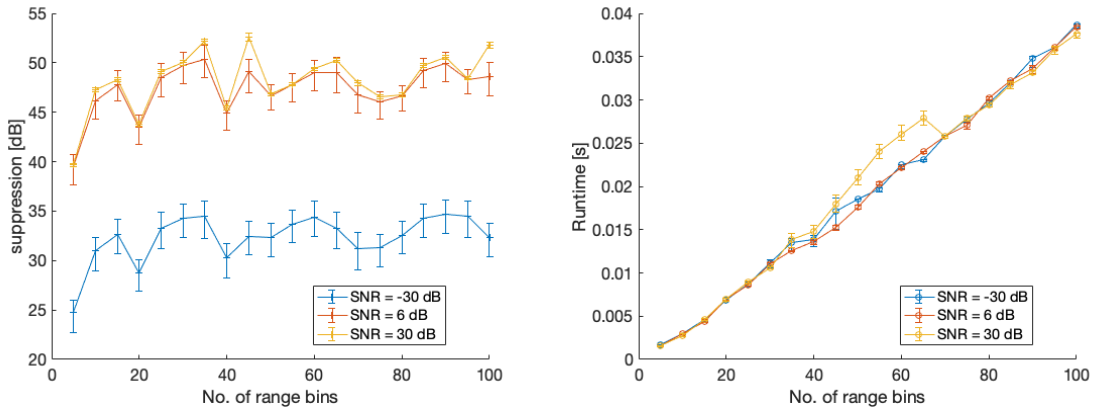

(a) LTE (b) DVB

Figure 28. ECA: Suppression and run time versus number of range bins, signal length = 7680

Figure 28 shows suppression and run time for against number of range bins, over

500 Monte Carlo trials for an LTE signal three symbols long. Similar results were obtained with different signal lengths for each signal type. There did not seem to be a consistent trend, and this may have been due to the implementation of the algorithm in MATLAB®. The suppression results for the ECA algorithm were consistently high, making the choice of range bins less complicated, and 50 delay bins were used in the algorithm.

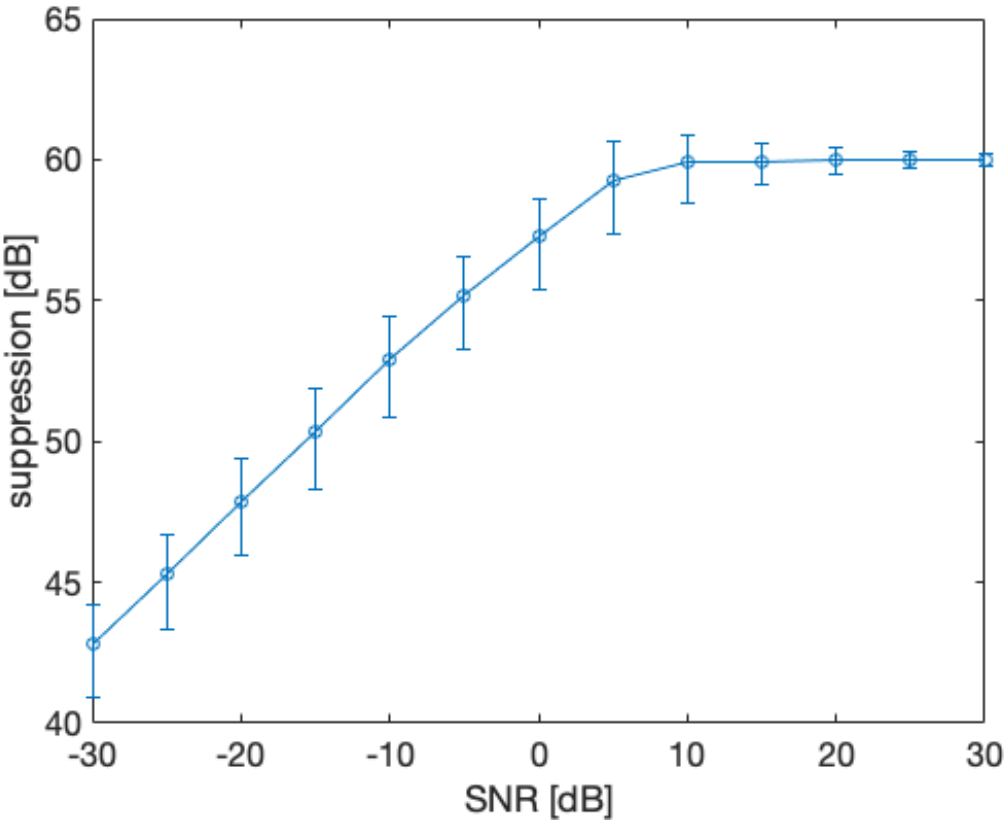

Figure 29. ECA performance with varying SNR

The performance of the ECA is shown in Figure 29 over 1000 trials, with error bars at the 25^{th} and 75^{th} percentiles. At a low SNR, suppression decreases by less than 20 dB from the suppression at the highest SNR tested, with a deviation of less than 2.5 dB either side of the mean. Like the Wiener filter, the deviation does not vary significantly below an SNR of 0 dB, which is a positive performance indicator.

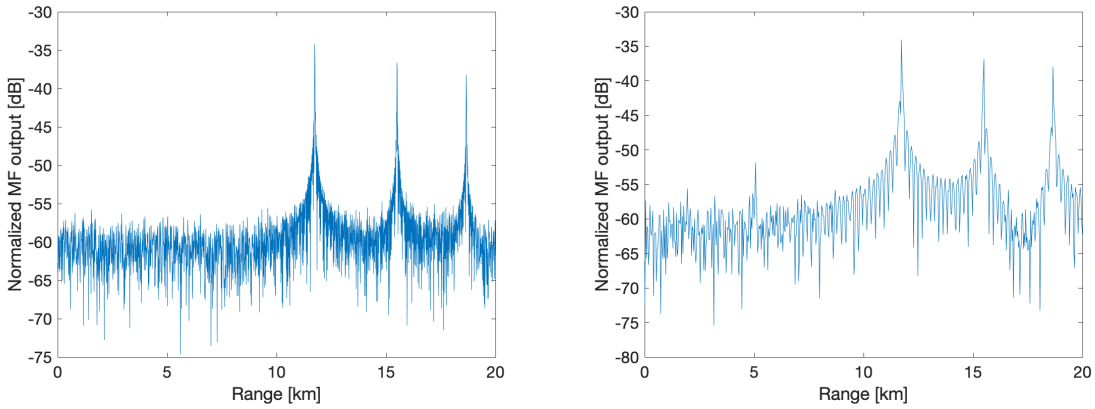

(a) LTE

(b) DVB

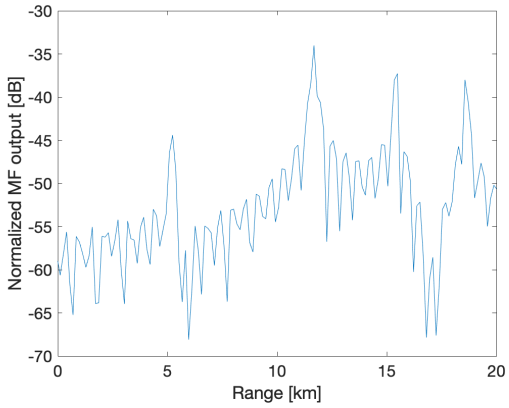

(c) DAB

Figure 30. Range profiles after applying ECA

4.3.3 Least Mean Squares.

The LMS algorithm is characterized by its simplicity and computational economy in that it is not required to compute correlations nor does it require matrix computations [20]. The main processes of the algorithm are a filtering process and an adaptive process. The tuneable parameters are the filter length, M, and the step size, μ.

The step size is selected such that [20]

$$0 < \mu < \frac{2}{MS_{max}}, \tag{49}$$

where S_{max} is the maximum value of the Power Spectral Density (PSD) [20]. The output of the algorithm is a filter estimate, $\underline{\hat{\mathbf{w}}}$, that is then convolved with the reference signal to give the estimated DPI signal. For every sample n, starting with the M^{th} sample, the inputs to the algorithm are an M-by-1 tap input vector,

$$\underline{\mathbf{u}}(n) = [u(n), u(n-1), ..., u(n-M+1)]^T \tag{50}$$

and the n^{th} sample of the desired signal, $d(n)$; the desired signal is the reference signal collected by the reference antenna. The filter estimate at sample $n+1$ is given by [20]

$$\underline{\hat{\mathbf{w}}}(n+1) = \underline{\hat{\mathbf{w}}}(n) + \mu \underline{\mathbf{u}}(n) e^*(n), \tag{51}$$

where

$$e(n) = d(n) - \underline{\hat{\mathbf{w}}}^H(n) \underline{\mathbf{u}}(n). \tag{52}$$

The final filter estimate is convolved with the reference signal, resulting in an estimate of the DPI signal. The estimated DPI has a delay proportional to the selected filter length, M. The delay is because the first $M-1$ samples of the surveillance signal are used to initiate the filter, with an initial filter estimate being a vector of zeros since no prior knowledge of the tap weight vector is available [20]. The implication of this is that a longer filter length relative to the length of the signal, the less of the signal is used to estimate the filter and therefore the less accurate the estimate. The level of

suppression achievable for a given set of external parameters depends on parameter selection, namely step size and filter length. The effect of filter length was found to vary with signal length, and was therefore more usefully defined as a proportion of the signal to ensure that it was long enough for effective suppression but not too long since only few tap weights were required to estimate the DPI signal.

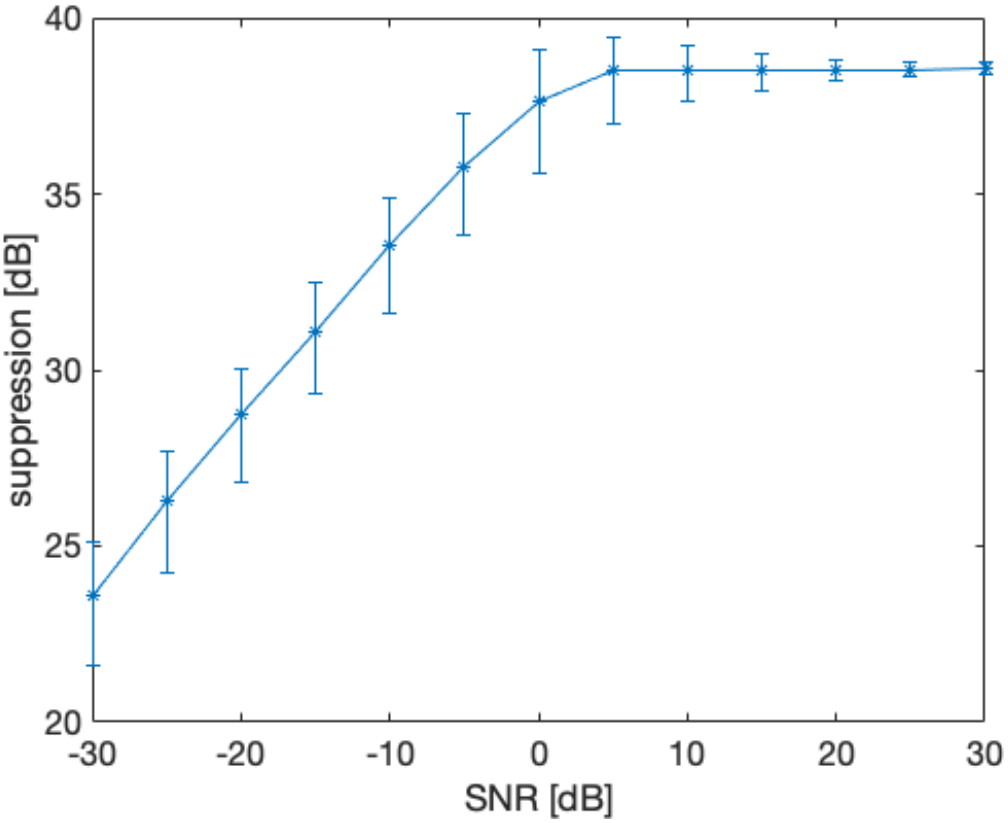

Figure 31. LMS performance with varying SNR

The performance of the LMS filter is shown in Figure 32 over 1000 trials, with error bars at the 25^{th} and 75^{th} percentiles. The best suppression is less than 40 dB, which means it would not be the best filter when the DPI is as high as 90 dB, which is possible [21]. The performance metrics shown are as for the Wiener and ECA filters.

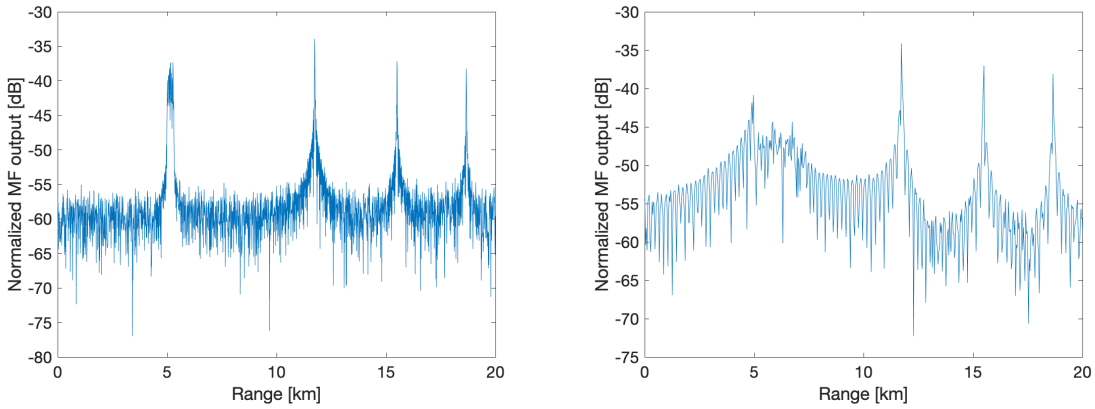

(a) LTE

(b) DVB

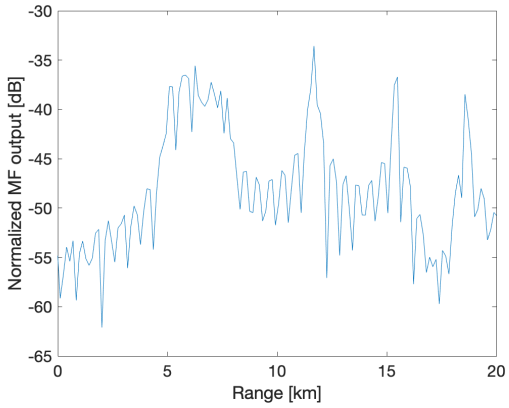

(c) DAB

Figure 32. Range profiles after applying LMS

4.3.4 Normalized Least Mean Squares.

The difference between LMS and NLMS is that the step size is normalized by the norm of the input vector. The filter estimate at sample $n+1$ is given by [20]

$$\underline{\hat{\mathbf{w}}}(n+1) = \underline{\hat{\mathbf{w}}}(n) + \hat{\mu}\underline{\mathbf{u}}(n)e^*(n), \tag{53}$$

where

$$\hat{\mu} = \frac{\mu}{||\underline{\mathbf{u}}(n)||}. \tag{54}$$

Again, step size and filter length were varied to determine the best values in terms of level of suppression and run time.

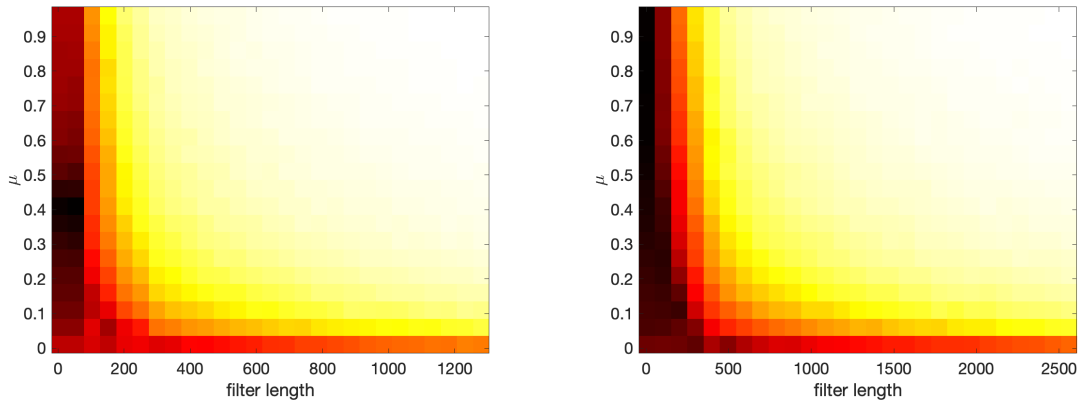

(a) signal length = 25600

(b) signal length = 51200

Figure 33. NLMS: suppression as a function of filter length and step size

From Figure 33, it can be seen that a short filter length results in the best estimation, and that the best step size depends on the signal length. Both parameters were determined from the input (surveillance) signal length, with $M = 0.01\%$ of signal length (or 5 for very short signals), and μ set at 0.2 since this value gave good results for longer signals, but for shorter signals a high value for μ gave poor results.

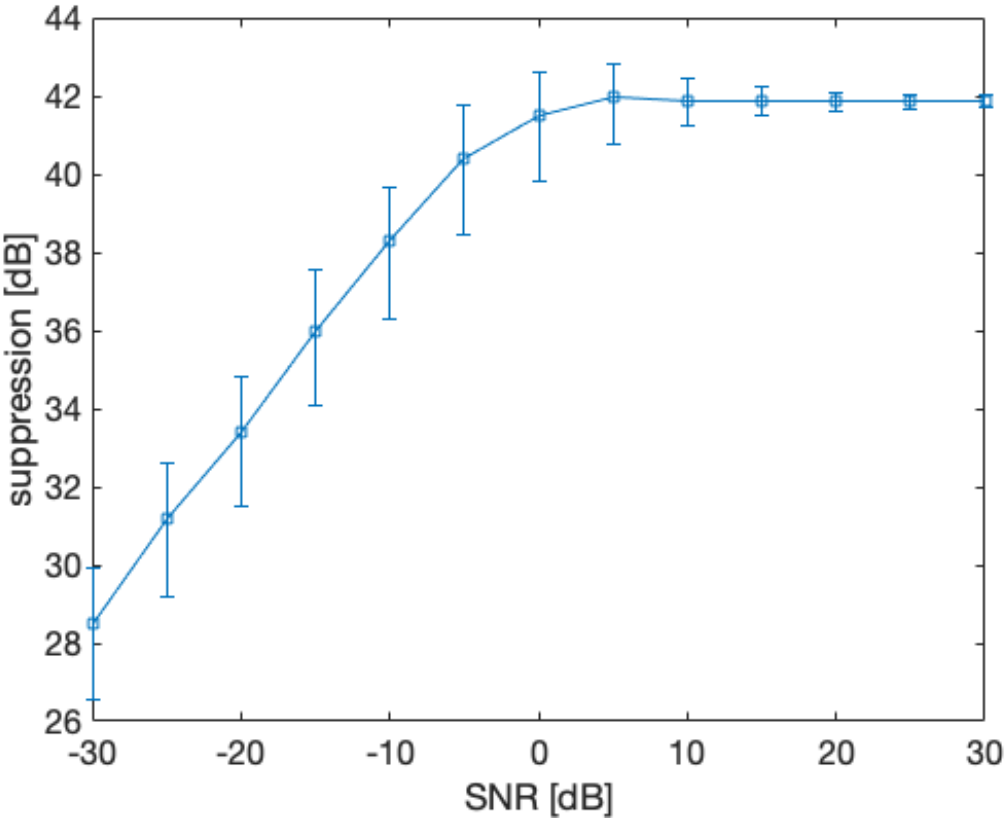

Figure 34. NLMS performance with varying SNR

The performance of the NLMS filter is shown in Figure 35 over 1000 trials, with error bars at the 25^{th} and 75^{th} percentiles. Suppression of over 42 dB is possible at high SNR values, making it better than the LMS filter in that metric. In addition, deviation from the mean at lower SNRs is slightly less than that for LMS.

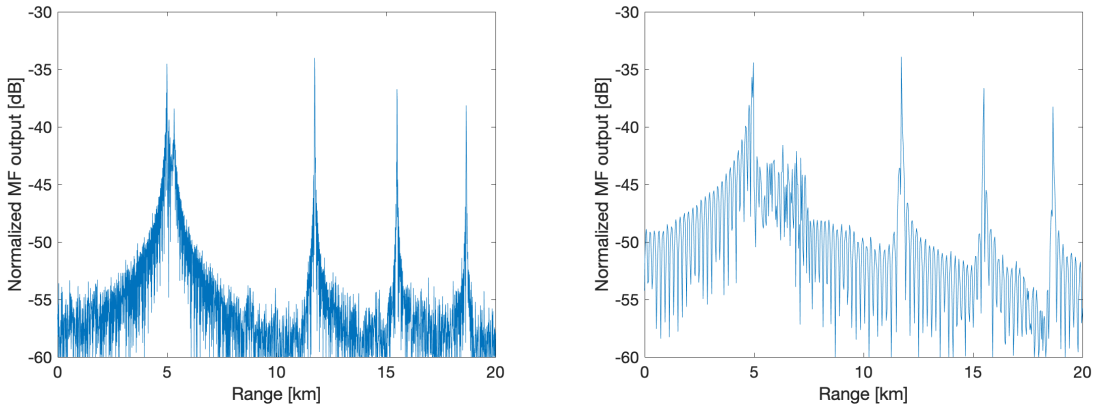

(a) LTE

(b) DVB

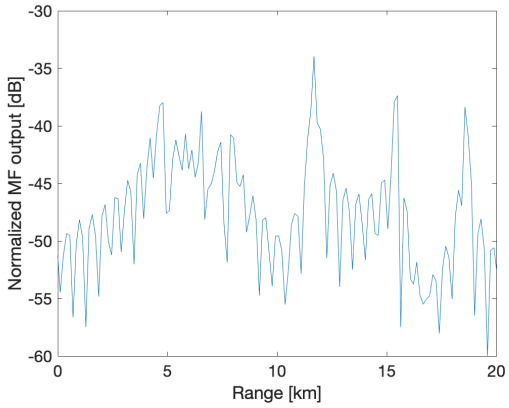

(c) DAB

Figure 35. Range profiles after applying NLMS

4.3.5 Fast Block Least Mean Squares.

In FBLMS filter parameters are updated in the frequency domain to take advantage of the fast convolution and correlation offered by the Fast Fourier Transform (FFT)[20]. The output equation is similar to that for LMS and NLMS; however, the generation of the filter tap weights is performed in the frequency domain. The first vector of filter tap weights, $\underline{\mathbf{W}}(0)$, is initialized as a $2M \times 1$ null vector since no information is known quantitatively about the system being estimated. The number of blocks is the length of the signal divided by the filter length, rounded down to the

nearest integer. For each block, k,

$$\underline{\mathbf{U}}(k) = \mathcal{F}\{\underline{\mathbf{u}}(n)\} \tag{55}$$

$$\underline{\mathbf{y}}(n) = \mathcal{F}^{-1}\{\underline{\mathbf{U}}(k) \circ \underline{\mathbf{W}}(k)\} \tag{56}$$

$\circ$ denotes the Hadamard product.

$$\underline{\mathbf{e}}(n) = \underline{\mathbf{d}}(k) - \underline{\mathbf{y}}(k) \tag{57}$$

$$\underline{\mathbf{E}}(k) = \mathcal{F}\{\begin{bmatrix}\mathbf{0}\\ \mathbf{e}\end{bmatrix}\} \tag{58}$$

$$\underline{\mathbf{P}}(k+1) = \gamma\underline{\mathbf{E}}(k) + (1-\gamma)|\underline{\mathbf{U}}(k)|^2 \tag{59}$$

$$\underline{\mathbf{D}}(k) = Diag(\underline{\mathbf{P}}^{-1}(k+1)) \tag{60}$$

$$\underline{\phi}(k) = \mathcal{F}^{-1}\{\underline{\mathbf{D}}(k) \circ \underline{\mathbf{U}}^*(k) \circ \underline{\mathbf{E}}(k)\} \tag{61}$$

$$\underline{\mathbf{W}}(k+1) = \underline{\mathbf{W}}(k) + \alpha\mathcal{F}\{\begin{bmatrix}\phi_{\mathbf{k}}\\ \mathbf{0}\end{bmatrix}\} \tag{62}$$

where

$$\underline{\mathbf{u}}(n) = [x(n), x(n-1), ..., x(n-M+1)]^T \tag{63}$$

and

$$\underline{\mathbf{d}}(n) = [d(n), d(n-1), ..., d(n-M+1)]^T \tag{64}$$

and $\underline{\mathbf{x}}(n)$ and $\underline{\mathbf{d}}(n)$ are the observed (surveillance) and desired (reference) signals respectively. α is an adaptation constant and γ is a forgetting factor, greater than zero and less than or equal to one [20]. $P(i)$ is an estimate of the power in the i^{th}

frequency bin; $\underline{\mathbf{P}}(0)$ was initialized as

$$\underline{\mathbf{P}}(0) = \underline{\delta}, \tag{65}$$

where each $\delta(i) = 0.1$ The FBLMS algorithm has more tuneable parameters - the adaptation constant, α, forgetting factor γ and number of FFT blocks, which is related to the filter length M. γ can be set to a value close to but not equal to one, while α can be set to $\alpha = 1/2M$.

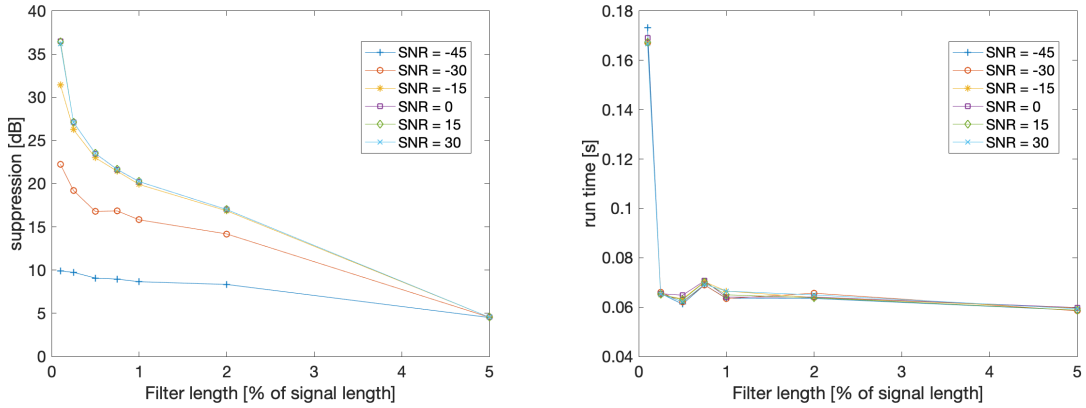

(a) Suppression as a function of filter length

(b) Run time as a function of filter length

Figure 36. FBLMS: Suppression and run time as a function filter length for LTE

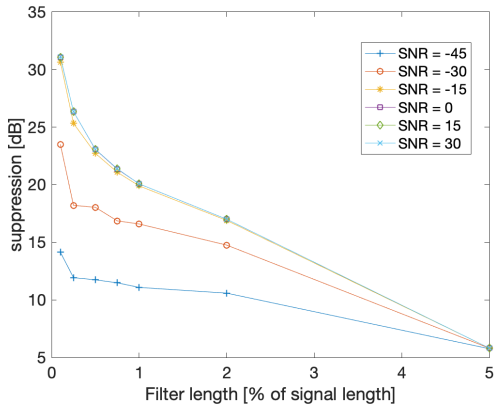

(a) Suppression as a function of filter length

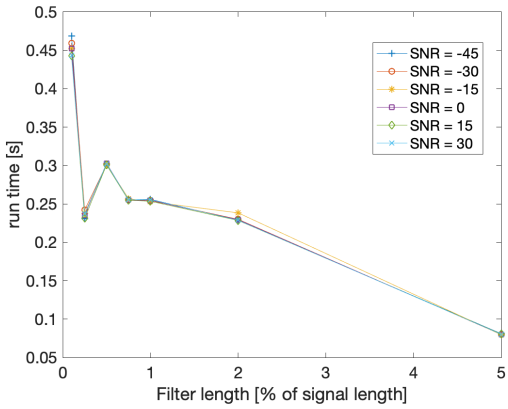

(b) Run time as a function of filter length

Figure 37. FBLMS: Suppression and run time as a function filter length for DVB

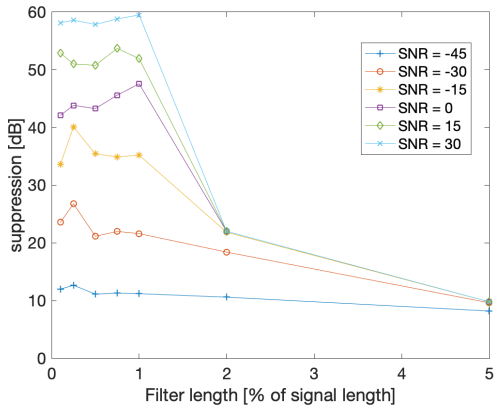

(a) Suppression as a function of filter length

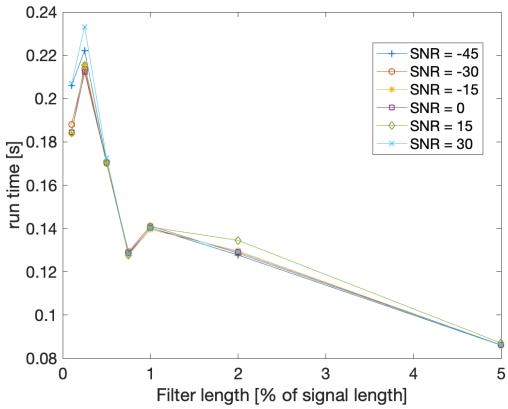

(b) Run time as a function of filter length

Figure 38. FBLMS: Suppression and run time as a function filter length for DAB

More blocks (shorter filter lengths) provided the best results, as shown in Figure **??**. M was set to 0.01% of signal length and α to $1/2M$. The value of γ found to produce the best results was 0.9.

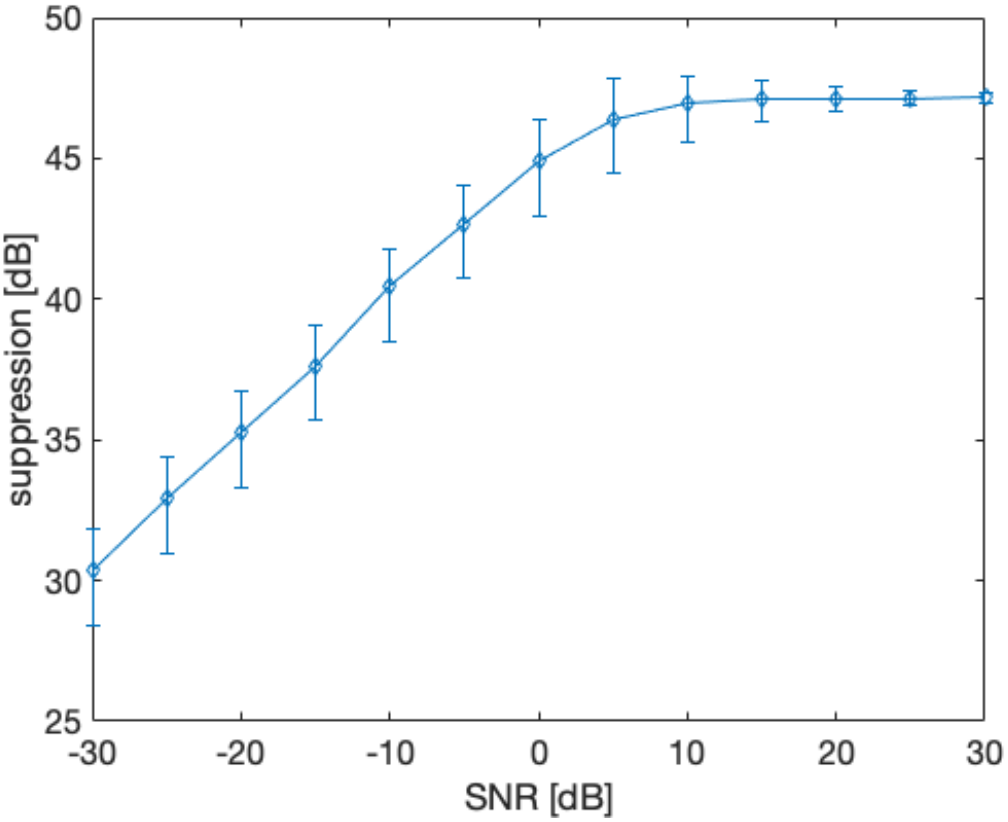

Figure 39. FBLMS performance with varying SNR

The suppression performance of FBLMS with varying SNR is shown in Figure 40, over 1000 trials. It does not stand out from LMS and NLMS in terms of total suppression and deviation; it has a lower run time as it is implemented in the frequency domain.

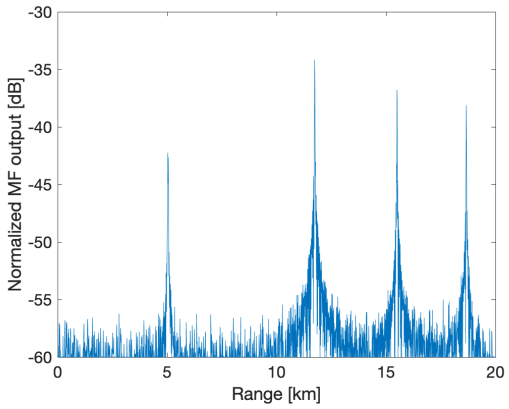

(a) LTE

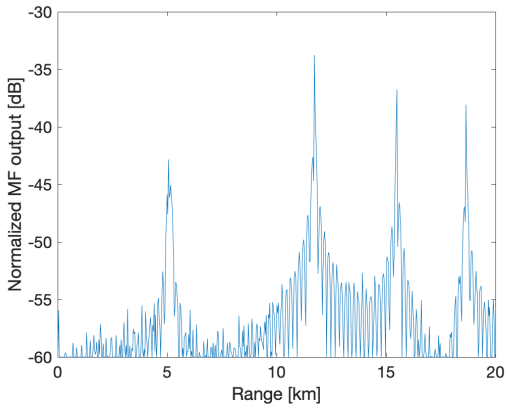

(b) DVB

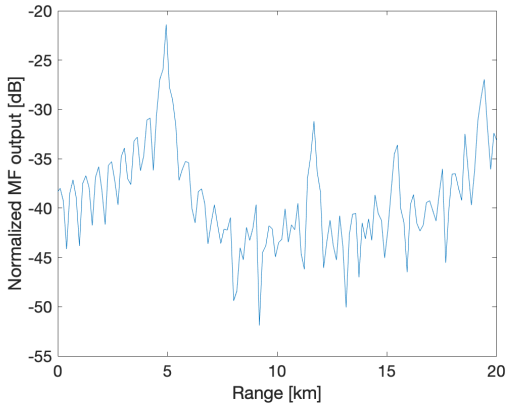

(c) DAB

Figure 40. Range profiles after applying FBLMS

4.3.6 Recursive Least Squares.

In the RLS algorithm, the computation of the filter estimate requires initial conditions, which are then iteratively updated as new information is input into the algorithm [20]. With initial inputs

$$\underline{\hat{\mathbf{w}}}(0) = \underline{\mathbf{0}} \tag{66}$$

$$\underline{\underline{\mathbf{\Phi}}}(0) = \delta^{-1}\underline{\underline{\mathbf{I}}}, \tag{67}$$

where $\underline{\underline{\mathbf{\Phi}}}$ is the $M \times M$ time-average correlation matrix of the input vector, $\underline{\underline{\mathbf{I}}}$ is the $M \times M$ identity matrix and M is the filter length and δ is the regularization parameter and is set to a small positive constant for high SNR and a large positive constant for low SNR. The regularization parameter is defined by [20]

$$\delta = \sigma_u^2 \mu^\alpha, \tag{68}$$

where σ_u^2 is the variance of the input vector, $\mu = 1 - \lambda$, λ is the forgetting factor, and is set to close to but not equal to unity and α is assigned a value corresponding to the SNR of the observed signal[20]. The values for α are 1 for high SNR (30 dB or more), ≤ -1 for low SNR (-10 dB or less) and $-1 \leq \alpha < 0$ for medium SNR values [20].

For each time instant n,

$$\underline{\mathbf{u}}(n) = [x(n), x(n-1), ..., x(n-M+1)]^T \tag{69}$$

$$\underline{\mathbf{k}}(n) = \frac{\lambda^{-1}\underline{\underline{\mathbf{\Phi}}}(n-1)\underline{\mathbf{u}}(n)}{1 + \lambda^{-1}\underline{\mathbf{u}}^H(n)\underline{\underline{\mathbf{\Phi}}}\underline{\mathbf{u}}(n)} \tag{70}$$

$$e(n) = d(n) - \underline{\hat{\mathbf{w}}}^H(n)\underline{\mathbf{u}}(n) \tag{71}$$

$$\underline{\hat{\mathbf{w}}}(n+1) = \underline{\hat{\mathbf{w}}}(n) + \underline{\mathbf{k}}(n)e^*(n) \tag{72}$$

$$\underline{\underline{\mathbf{\Phi}}}(n+1) = \lambda^{-1}\underline{\underline{\mathbf{\Phi}}}(n) - \lambda^{-1}\underline{\mathbf{k}}(n)\underline{\mathbf{u}}^H(n)\underline{\underline{\mathbf{\Phi}}}(n). \tag{73}$$

$\underline{\mathbf{k}}$ is a gain vector by which the old value of the estimated filter is incremented to get the new value. Parameter selection for RLS was relatively straightforward, since filter length was the only parameter to be picked rather than computed. The filter length was varied and the level of suppression and run time computed for different SNR values in order to determine suitable filter length values.

It was found that keeping the filter length below 0.5% of signal length resulted in

good suppression while keeping the run time relatively low. A filter length of 0.01% of the signal length was selected for simulations in this thesis.

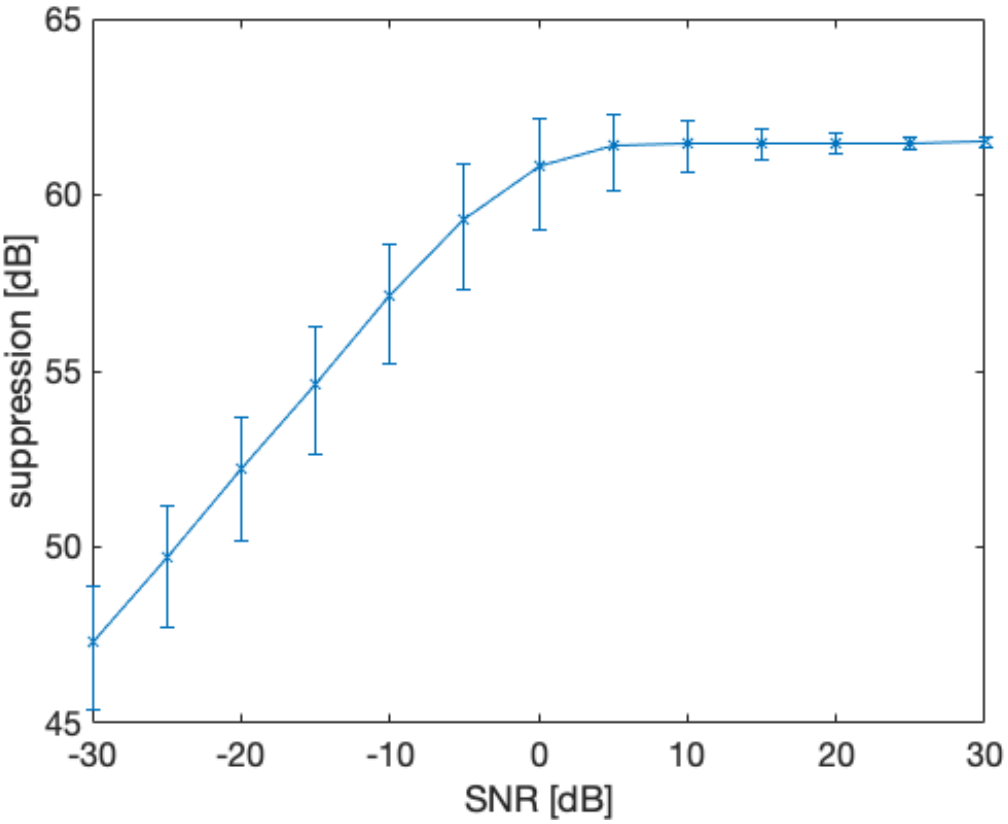

Figure 41. RLS performance with varying SNR

The suppression performance of the RLS algorithm was tested over 1000 trials for varying SNR values (Figure 42). RLS performed better in terms of total suppression and deviation than the mean squares algorithms, however it did have the longest run time of all the algorithms. RLS would be suitable where an adaptive filter is required due to unknown or varying signal statistics, and performance was more important than time, for example SAR imaging done in post processing.

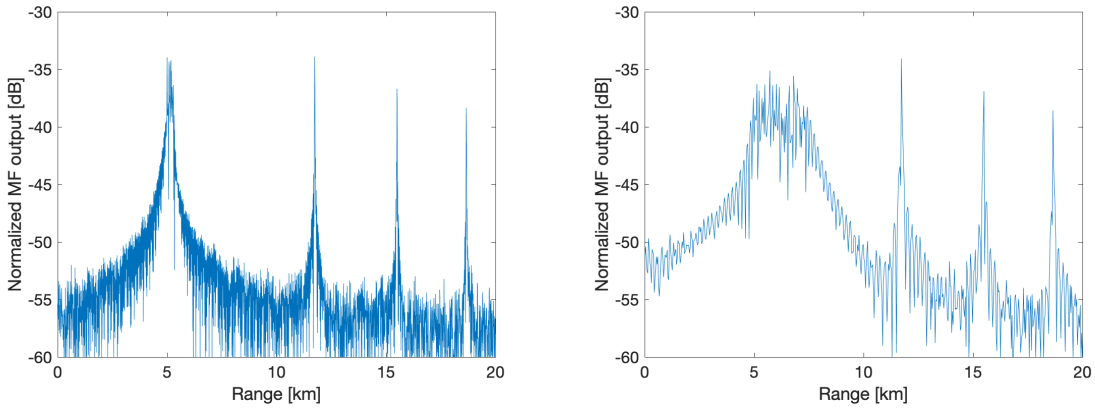

(a) LTE

(b) DVB

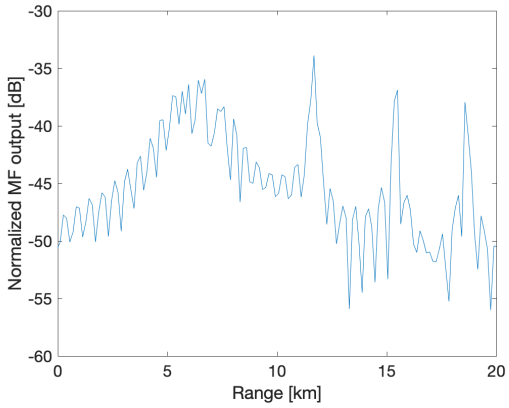

(c) DAB

Figure 42. Range profiles after applying RLS

4.4 Comparison of Algorithms

In [3] the algorithms discussed were compared via simulation and experiment using a DVB signal. The comparison was based on error (between computed and actual filter coefficients), convergence time and SCR. The authors concluded that all algorithms tested were able to effectively cancel the direct signal. They resulted in very similar SCR, but the RLS algorithm far outperformed the other algorithms on error and convergence time; it was however found to be relatively computationally

complex. A comparative analysis of adaptive filtering algorithms for DPI suppression is presented in [23], in which a commercial FM signal was used. The conclusion of [23] was that the algorithms performed sufficiently in terms of clutter cancellation and target detection. The findings of previous works may not necessarily be reproducible under different simulation conditions or real time application, but they provide a point of comparison for this work.

The results from Section 4.3 show that algorithm parameters may be best selected based on the signal length, rather than arbitrarily picked. For all algorithms, run time increased with filter length, with the exception of FBLMS, where run time increased with number of blocks, which is inversely proportional to filter length since the number of blocks is equal to N/M, where N is the signal length and M is the filter length.

Table 6. Suppression algorithm parameters

Suppression algorithm	**Parameters**
Wiener	M = 0.0001N
ECA	range bins = 50
LMS	M = 0.0001N $\mu = \mu_{max}/2$ $\mu_{max} = 2/MP_{surv}$
NLMS	M = 0.0001N $\mu = 0.2$
FBLMS	M = 0.0001N $\alpha = 1/2M$ $\gamma = 0.9$
RLS	M = 0.0001N $\lambda = 0.9999$

Parameters for the algorithms were selected from the results in Section 4.3 and are summarized in Table 6. In the table P_{surv} is the power of the surveillance signal, which was used to determine the upper limit of the step-size, μ; μ was arbitrarily set to half of the maximum value computed. The suppression performance of the algorithms was compared for varying SNR values, and for each signal type.

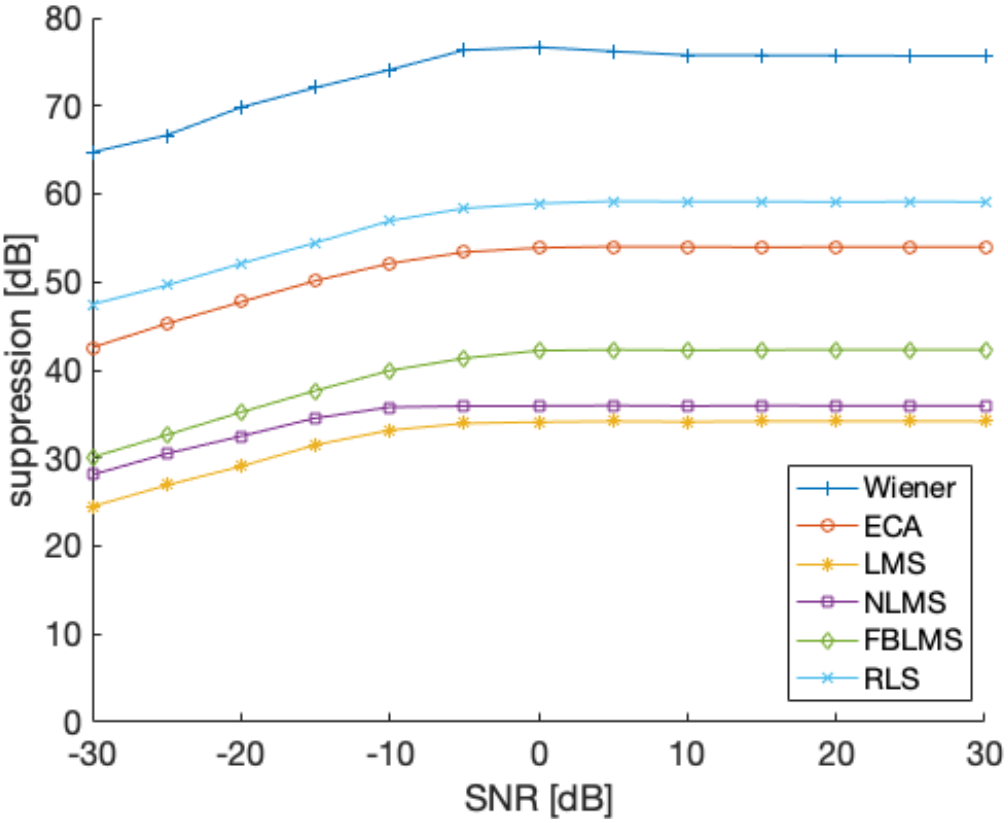

Figure 43. Suppression versus SNR

Figure 43 shows suppression performance with increasing SNR with no clutter present in the surveillance and reference channels. 500 Monte Carlo trials were run and the mean suppression computed and plotted.

The level of suppression does not directly translate to effectiveness in target detection; the SCR did not have a significant effect on the level of suppression achieved, but had an effect on target detection, since clutter was modelled as point targets,

whose echoes also produce a matched filter response, that is, the clutter mimics real targets.

4.5 Chapter conclusion

DPI suppression algorithms were presented and their performance analyzed and tested through simulation. All algorithms were found to be sufficient at suppressing DPI, with the level of suppression being the limiting factor of each in how effective it would be under different circumstances. It should be noted that the results of simulations to select parameters for the algorithms were specific to suppressing the DPI term, and therefore fewer filter tap weights were required to estimate the DPI signal; however, filter length is related to the number of tap weights of the system to be estimated and therefore these results would not necessarily hold for clutter suppression with a high number of clutter coefficients. In addition a longer surveillance and reference signal would provide better tap weight estimates than shorter signals, though this was not explored.

V. REFERENCE SIGNAL PROCESSING

The structure of OFDM signals results in ambiguity functions that have peaks other than at zero delay and Doppler. The reference signal can be processed to cancel range ambiguities due to signal structure. The resulting signal is then used to build a matched filter that results in the correct range profile.

5.1 Range and Doppler ambiguity cancellation

After DPI cancellation, the resulting signal is made up of target echoes and noise. While the MF output no longer contains a response from the direct signal, it will still contain cyclic prefix peaks from each of the targets. In a SAR imaging scenario, the surveillance signal contains a continuum of target echoes of varying signal strength based on their bistatic range, RCS and atmospheric losses. While the range and power level of the CP peaks relative to the main peak are known, the main peak of targets relative to each other is not known. The net result is that it may not be possible to distinguish between actual target peaks and CP peaks of other targets and be missed due to not being able to be distinguished from CP peaks of other targets.

The least complex way of solving the CP problem is limiting the range within which targets of interest lie to within the unambiguous range. If the detection range of interest is less than the CP range, it can be ignored with no processing necessary [25]. Referring to Table 3, while DAB and DVB signals have large unambiguous ranges relative to LTE signals, they are usually high power signals in order to reach audiences in geographically wide areas: 1 - 10 kW for DAB and 10 - 100 kW for DVB [26]. Though their range resolution is relatively coarse, they can be employed in imaging of large areas such as major highways, tracking variations in fields, coast lines, large city outlines and mountain outlines [27]. The high power offered by DVB

and DAB signals allows for larger bistatic baselines, such as those in the experimental set up in [11] of up to 157 km. The high power of the signals, however, also means that echoes from clutter at ranges beyond the range of interest could present interference via their leading CP peaks, which could occur within the range of interest and appear as target echoes. LTE signals provide a better range resolution, but they have a smaller CP range, which could result in interference from CP peaks depending on the geometry. Coverage cell sizes up to 100 km are possible [28]; and with a CP range of 20 km, it would make sense to process out CP peaks in order to take advantage of these signals and have flexibility in terms of bistatic geometries.

Due to the opportunities offered by OFDM signals for passive radar and the numerous potential geometries, it makes sense to make passive radar receivers as flexible as possible via signal processing to cancel interference and mitigate the effects of range ambiguities. Several works have addressed the problem of ambiguities due to OFDM signal structures and presented methods to mitigate them. References [29] and [30] proposed AF improvement methods for DVB, which included methods for removing the CP peak which can be applied to any OFDM signal with a CP.

5.2 Cyclic prefix cancellation

Cancelling the effect of the CP would make OFDM-based passive radar more flexible. The method of removing the CP peaks in the output of the matched filter is to process the reference signal so that it does not correlate with the surveillance signal during the CP interval. This was accomplished in [29] and [30] by setting the CP and the portion of the signal from which the CP data is taken to zero. The resulting MF does not result in peaks due to the CP and CP data. This was implemented successfully for an example scenario.

A MATLAB® simulation was used to illustrate the effects of DPI and CP on MF

output and the resulting range profiles, and thus by extension on SAR images. The values used may not necessarily depict a practicable real world scenario but have been picked so as to effectively aid the discussion on DPI and range ambiguities. A possible scenario would be imaging an airstrip or small town in a low population density area, where the LTE transmitter coverage range could be up to 100 km; LTE is able to support cell sizes up to and beyond 100 km [28]. The large illumination area would allow for flexibility in the positioning of the receiver, for example, the receiver could be close to the transmitter in order to get as clean a reference signal as possible, while the scene could be far relative to the bistatic baseline resulting in a small bistatic angle as well as a more covert operation. The signal used to illustrate CP cancellation was an FDD LTE DL signal with an extended CP.

Table 7. Simulation parameters

	Bistatic range [km]	Leading CP range [km]	Trailing CP range [km]
Baseline	1	-19	21
Target 1	18	-2	38
Target 2	26	6	46
Target 3	42	22	62

The geometry and simulation parameters are as shown in Table 7. The ECA algorithm was implemented for DPI suppression.

After effectively suppressing the DPI, the CP peaks were cancelled by modifying the MF reference signal so as to null the CP and CP data portion of each symbol, leaving only the unique part of the symbol, as proposed in [29] and [30]. Figure 44(a) shows the location of the target peaks and CP peaks in the range profile, while Figure 44(b) shows the range profile before DPI suppression. It can be seen in Figure

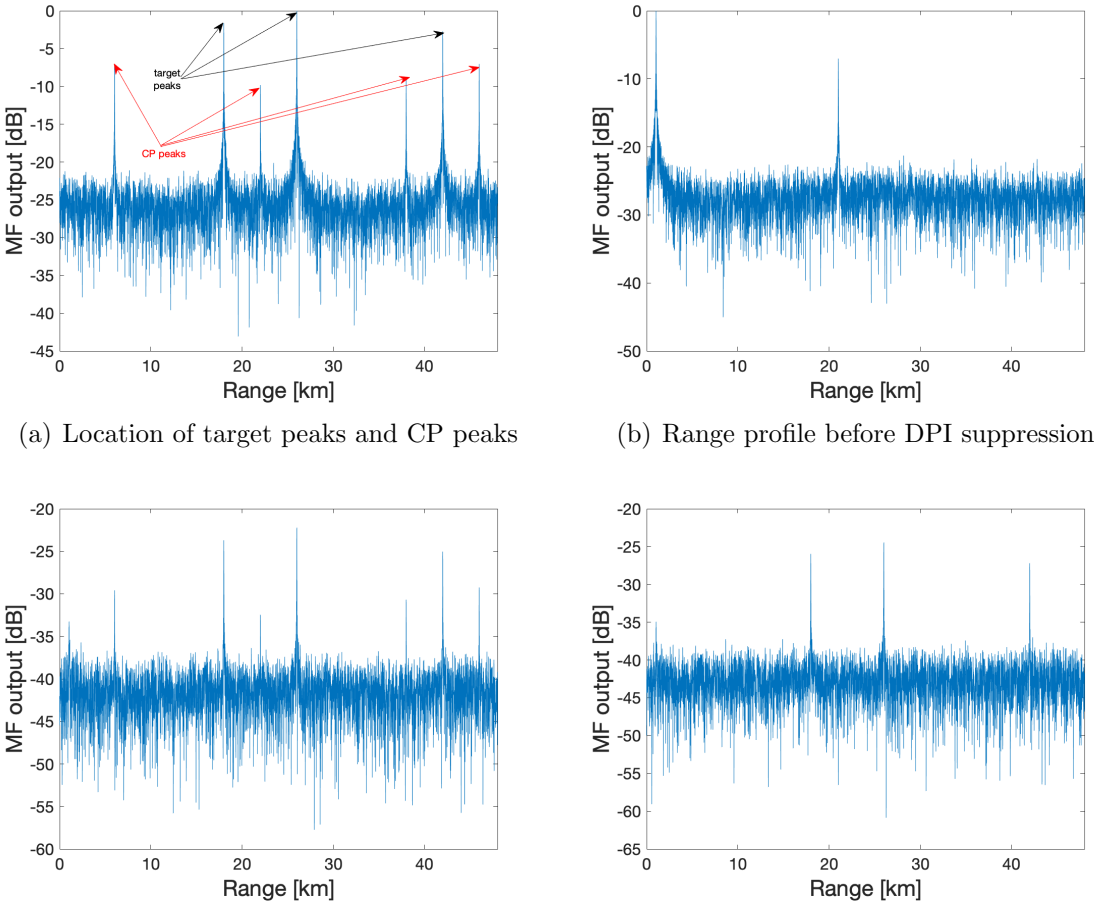

(a) Location of target peaks and CP peaks

(b) Range profile before DPI suppression

(c) After DPI suppression

(d) Effect of CP on range profile

Figure 44. Effect of CP on range profile

44(b) that the direct signal and its CP dominate and mask the targets in the range of interest. After DPI suppression, the targets can be detected; however, their CP peaks are also present in the range profile. Target 1's trailing CP is at a range of 38 km and target 3's leading CP is at a range of 22 km; since the range of interest is 15 km - 45 km, the CP peaks appear as targets (Figure 44(c)). Figure 44(d) shows the AF and range profile after CP cancellation, with only the true target peaks.

5.3 Cancellation of range ambiguities in DVB

Range ambiguities occur in the DVB SAF due to scattered pilots before the CP peak; from (19), scattered pilot peaks occur every 22.4 km, while the CP peaks occurs at a range of 268.8 km. It is therefore useful to cancel the scattered pilot ambiguities in order to extend the unambiguous range beyond 22.4 km. Since the scattered pilots are transmitted at a boosted power level (hence the appearance of the peaks in the SAF) in a periodic pattern, setting them to zero would retain the periodicity. To cancel the ambiguities due to scattered pilots, they are equalized to the power of data-carrying subcarriers [18]. Ambiguities due to continual pilots occur beyond the CP prefix since their pattern repeats every frame rather than every symbol; these ambiguities are cancelled by nulling the continual pilot subcarriers [18].

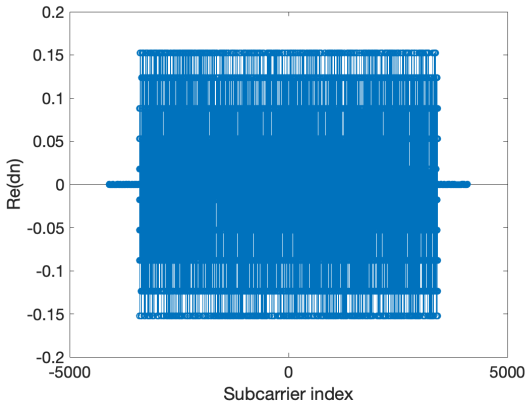

(a) D_ns for one symbol

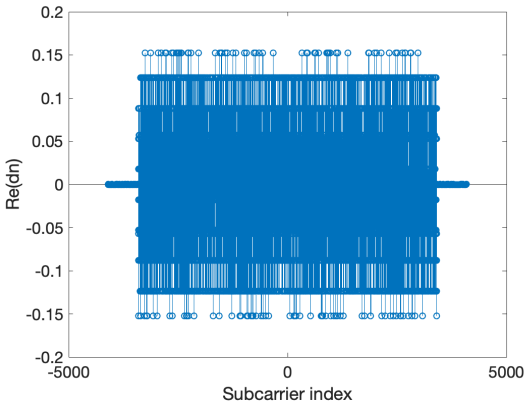

(b) D_ns for one symbol - scattered pilots equalized

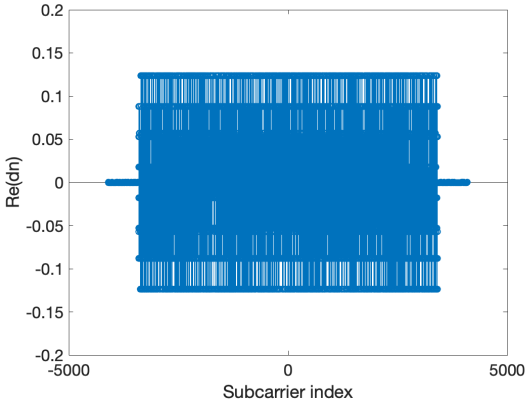

(c) D_ns for one symbol - continual pilots nulled

Figure 45. Pilot equalization and nulling

The process of cancelling ambiguities due to pilot signals is shown in Figure 45; Figure 45(a) shows the spectrum for one symbol, with pilot subcarriers at the highest amplitudes, Figure 45(b) shows the spectrum after the scattered pilots have been equalized down (continual pilots can be seen standing out above the rest of the subcarriers). Finally in Figure 45(c), the continual pilots have been nulled.

A scenario is used to show the effect of range ambiguities due to pilots, and the effectiveness of the described cancellation method, where there are three targets and

peaks due to pilot signals are expected to occur within the range of interest.

Table 8. DVB range ambiguity scenario distances

L [km]	10
R_1 [km]	24.94
R_2 [km]	48.20
R_3 [km]	72.98

Table 8 shows the bistatic range and target ranges.

Peaks due to scattered pilots can be seen in Figure 46(a), with the first one at $L+22.4$ km, and two more spaced at 22.4 km from each other. After DPI suppression, these peaks are cancelled as they are due to the direct signal, but there are now scattered pilot peaks due to the targets. After equalization of scattered pilots, the correct range profile is obtained, with target peaks only.

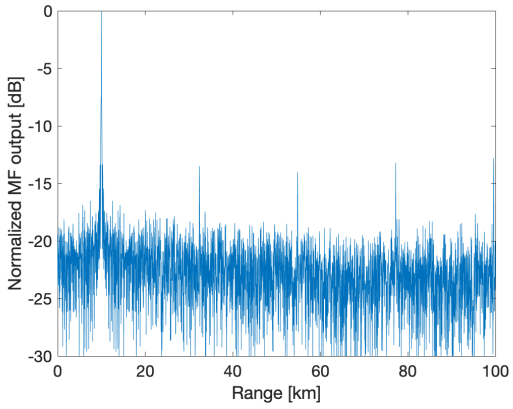

(a) No DPI suppression - DPI peak and range ambiguities

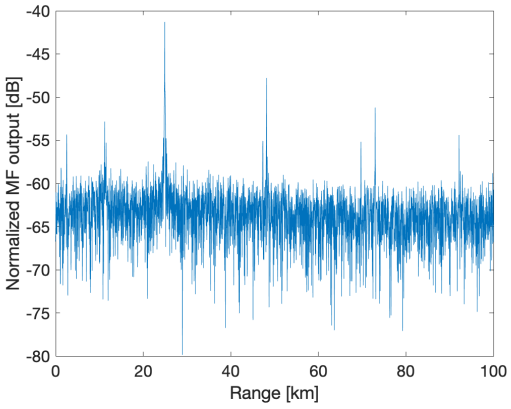

(b) After DPI suppression - ambiguities from targets present

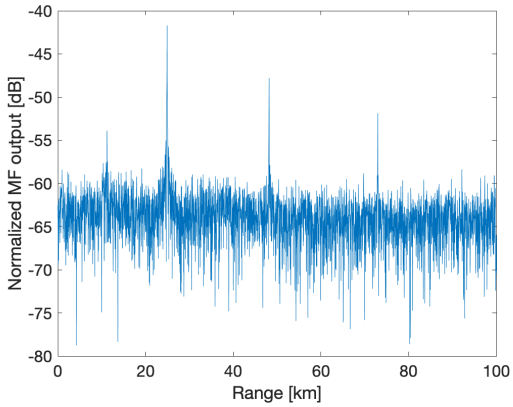

(c) After DPI suppression - ambiguities cancelled

Figure 46. DVB range ambiguity effect and cancellation

5.4 Effect of DPI on SAR images

Having shown the effect of DPI on a single range profile, the effect of DPI on a SAR image is now considered. Forming the correct image in SAR requires that the correct range profile be obtained from each slow time sample, that is, from every position of the receiver.

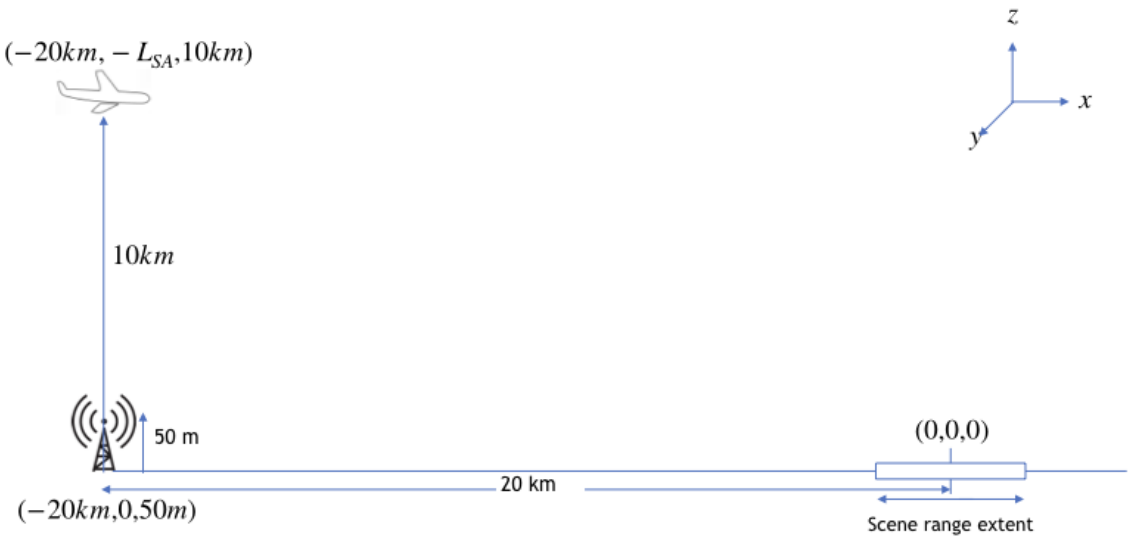

Figure 47. SAR imaging scene

Figure 47 shows the collection geometry. There is one target at scene center, which is at co-ordinates $(0, 0, 0)$. L_{SA} is the synthetic aperture length.

In the scenario, spotlight SAR is simulated, in which echoes from the scene are collected from different angles (receiver location) and coherently combined. Each received pulse is processed through a matched filter, and the data thus formed is the scene's phase history data. In this section, pulse refers to a single OFDM symbol or a number of OFDM symbols considered for each slow time sample. In the scenario simulated, an LTE pulse consisted of three symbols, while for DAB and DVB, one symbol was considered a pulse. The pulse duration therefore was for 0.25 ms LTE, 1.1 ms for DVB and 1.2 ms for DAB.

Due to the simplicity of the scenario, the move-stop-move receiver motion was not computed in a realistic sense, rather it was assumed that the platform would receive a pulse at each position for a total of 800 pulses. This assumption would not necessarily hold for a real life scenario, but was found sufficient for the purposes of the simulation, whose aim was to show the effect of DPI on the image and that DPI suppression is possible and effective in passive SAR.

The direct path signal was modeled as a delayed copy of the transmitted signal scaled to 30 dB above the target echo signal. The direct signal delay for each pulse was computed as

$$\tau_p = \frac{L_p}{c} \tag{74}$$

where L_p was the bistatic baseline at each receiver position. The DPI signal was then added to each received signal at each receiver position. An image was formed using the phase history to show the effect of DPI.

The ECA algorithm was then applied to each received pulse, and the phase history used to form an image to show the effectiveness of DPI suppression.

For the simulation, noise and clutter were not added, as the aim was to show the effect of DPI only.

The range and cross range resolutions, ΔR and ΔCR are given by [1]

$$\Delta R = \frac{c}{2B\cos(\frac{\beta}{2})} \tag{75}$$

$$\Delta CR = \frac{c}{4f_c \sin(\frac{\Delta\phi}{2})\cos(\theta_b)\cos(\frac{\beta}{2})} \tag{76}$$

were $\Delta\phi$ is the azimuth extent

Table 9. Range and cross range resolutions

Signal	**Carrier frequency [MHz]**	**Effective bandwidth [MHz]**	**Range resolution [m]**	**Cross range resolution [m]**
LTE	728	19.815	7.56	2.84
DVB	474	7.608	19.7	4.36
DAB	47	1.537	97.53	43.96

Table 9 shows the range and cross range resolutions for the three signals used. The phase history is given by [31]

$$G_p[U_n] = S_{surv}[n]S^{'}_{ref}[n] \tag{77}$$

where $G_p[U_n]$ is the 1D Discrete Fourier Transform (DFT) of the scene reflectivity function of the p^th pulse, U_n is the spatial frequency variable and $S_{surv}[n]$ is the spectrum of the received signal on the surveillance channel. $S^{'}_{ref}[n]$ is the pseudoinverse of the spectrum of the reference signal delayed to scene center, where

$$S^{'}_{ref}[n] = \frac{S^{*}_{ref}[n]}{|S_{ref}[n]|^2}, \qquad \text{if} \quad S_{ref}[n] \neq 0 \tag{78}$$

$$S^{'}_{ref}[n] = 0, \qquad \text{if} \quad S_{ref}[n] = 0 \tag{79}$$

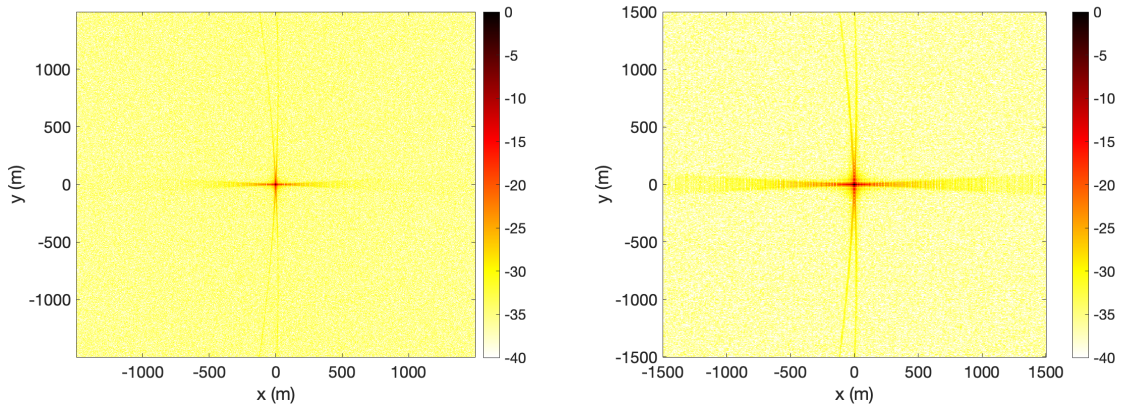

(a) LTE

(b) DVB

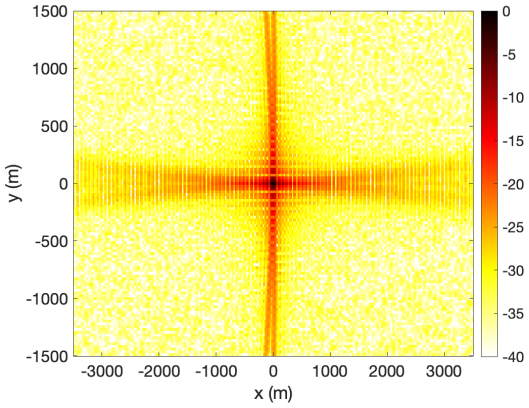

(c) DAB

Figure 48. Image with no clutter, no noise and no DPI present

Figure 48 shows the images formed with no DPI present, forming the baseline image.

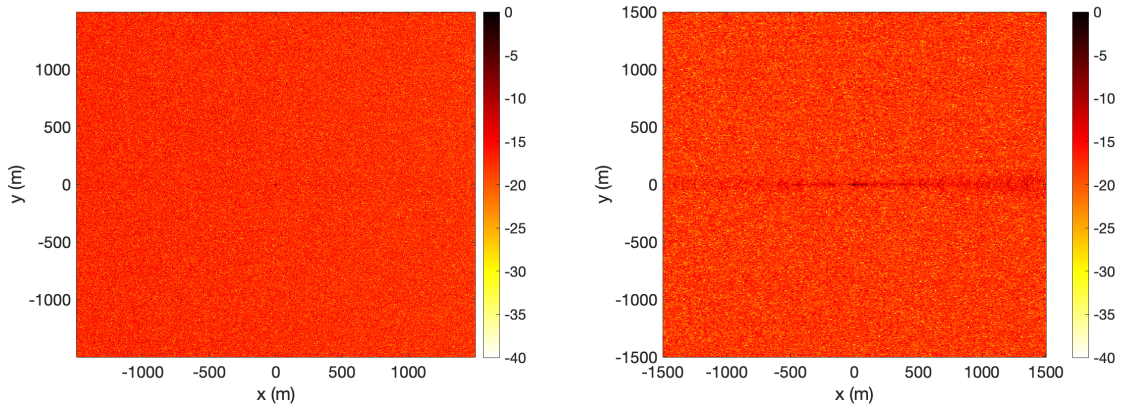

(a) LTE

(b) DVB

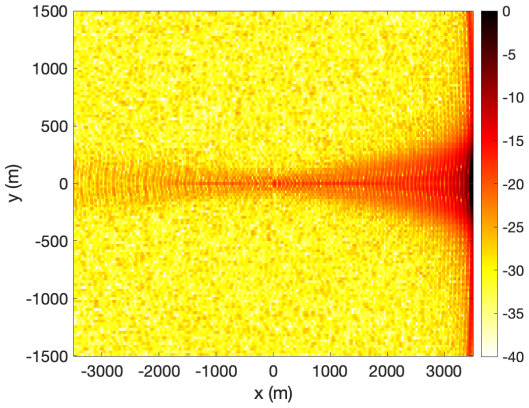

(c) DAB

Figure 49. Images with DPI - no suppression

Figure 49 shows the images with DPI present and no suppression.

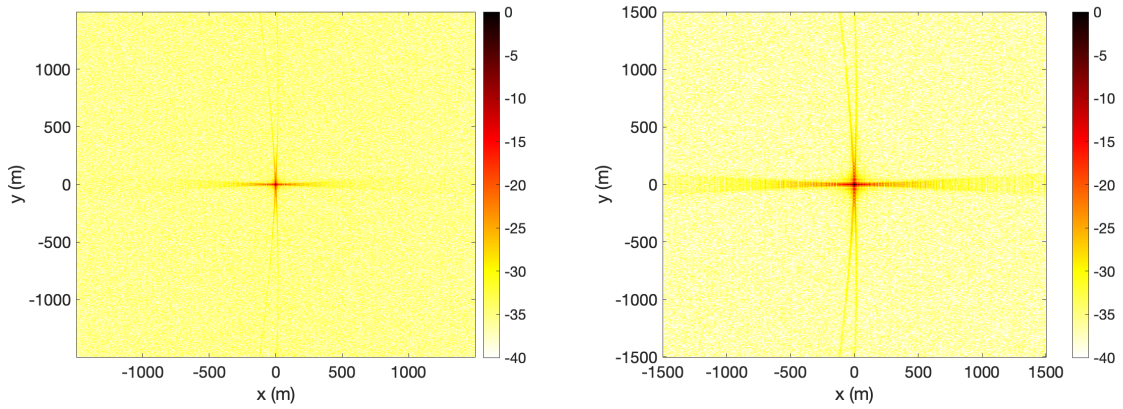

(a) LTE

(b) DVB

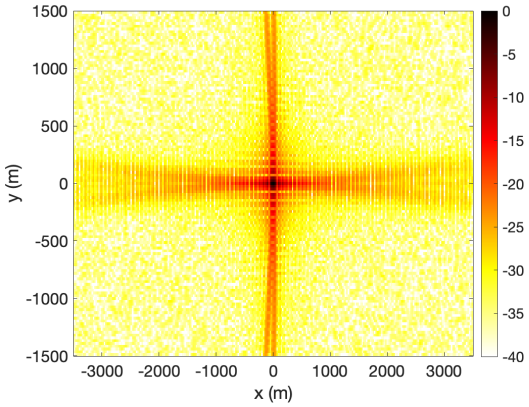

(c) DAB

Figure 50. Images after suppression

Figure 50 are the resulting images after DPI suppression, showing that it was effective.

5.5 Chapter conclusion

Reference signal processing to cancel range ambiguities were successfully implemented. A SAR imaging scenario was simulated in order to explore the effect of DPI on SAR images, and the effectiveness of DPI cancellation on the resulting image.

VI. Conclusion

This thesis aimed at providing a consolidated look at aspects of PBR that have been hitherto considered in isolation - the problem of DPI, the properties of OFDM signals and their implications when applied in passive radar. The structure of OFDM signals was analyzed in order to understand their implications on range profiles and by extension SAR images formed by processing these range profiles. DPI was defined and its effect in passive radar was discussed. Methods of DPI mitigation and suppression in literature were reviewed, with the conclusion that signal processing methods were necessary in order to take full advantage of passive radar. Six DPI suppression algorithms were analyzed, and the best parameters were determined. The algorithms were then implemented and analyzed for performance, and applied to LTE, DVB and DAB signals successfully. The algorithms were able to be implemented so as to be flexible, by allowing for parameter selection based on input signal.

Processing was applied to the reference signal in order to mitigate the effects of OFDM signal structure, and were shown to be effective using simple scenarios. Finally, the effect of DPI on SAR imaging was explored, as well as the effectiveness of DPI suppression in the resultng image.

6.1 Future work

This research readily extends to experimental work to test the performance of the DPI suppression algorithms, and whether the parameter selection criteria are valid or were only valid in the specific simulations in this work. It would be of interest to extend the experimental SAR imaging work done at AFIT [7] to include DPI in the surveillance signal and verify what effect it has on the resulting images, as well as test the DPI suppression algorithms on real data.

Bibliography

1. Aaron Evers and Julie Ann Jackson, "Analysis of an LTE waveform for radar applications," in *IEEE National Radar Conference - Proceedings*, 2014, vol. 1, pp. 200–205.

2. European Telecommunications Standards Institute, "Digital Video Broadcasting (DVB); Framing structure, channel coding and modulation for digital terrestrial television," *Technical Specification*, vol. 0, pp. 9, 2004.

3. Joseph Landon Garry, Chris J. Baker, and Graeme E. Smith, "Evaluation of direct signal suppression for passive radar," *IEEE Transactions on Geoscience and Remote Sensing*, vol. 55, no. 7, pp. 3786–3799, 2017.

4. N. J. Willis, *Bistatic Radar*, Scitech, Rayleigh, NC, 2005.

5. M. A. Richards, J. A. Scheer, and W. A. Holm, *Principles of Modern Radar: Basic Principles*, Scitech, , 2010.

6. M. I. Skolnik, *Radar Handbook*, McGraw-Hill, 2008.

7. Aaron Evers and Julie Ann Jackson, "Experimental passive SAR imaging exploiting LTE, DVB, and DAB signals," *IEEE National Radar Conference - Proceedings*, pp. 680–685, 2014.

8. R.S.A. Raja Abdullah, N.H. Abdul Aziz, A. Ismail, F. Hashim, and A.A. Salah, "Experimental study of LTE signals as illuminators of opportunity for passive bistatic radar applications," *Electronics Letters*, vol. 50, no. 7, pp. 545–547, 2014.

9. Raja Syamsul Azmir Raja Abdullah, Fazirul Hisham Hashim, Asem A. Salah, Nur Emileen Abdul Rashid, Alyani Ismail, and Nor Hafizah Abdul Aziz, "Experimental investigation on target detection and tracking in passive radar using long-term evolution signal," *IET Radar, Sonar & Navigation*, vol. 10, no. 3, pp. 577–585, 2016.

10. James E. Palmer and Stephen J. Searle, "Evaluation of adaptive filter algorithms for clutter cancellation in Passive Bistatic Radar," *IEEE National Radar Conference - Proceedings*, pp. 0493–0498, 2012.

11. C. R. Berger, B. Demissie, J. Heckenbach, P. Willett, and S. Zhou, "Signal processing for passive radar using ofdm waveforms," *IEEE Journal of Selected Topics in Signal Processing*, vol. 4, no. 1, pp. 226–238, Feb 2010.

12. Aaron Evers and Julie A. Jackson, "Cross-ambiguity characterization of communication waveform features for passive radar," *IEEE Transactions on Aerospace and Electronic Systems*, vol. 51, no. 4, pp. 3440–3445, 2015.

13. 3GPP, "TS 36.211 version 10.0.0 Release 10; Evolved Universal Terrestrial Radio Access (E-UTRA); Physical channels and modulation," *Technical Specification*, vol. 0, pp. 9, 2011.

14. J. R. Gutierrez Del Arroyo and J. A. Jackson, "Wimax ofdm for passive sar ground imaging," *IEEE Transactions on Aerospace and Electronic Systems*, vol. 49, no. 2, pp. 945–959, APRIL 2013.

15. D. Gromek, K. Kulpa, and P. Samczyski, "Experimental results of passive sar imaging using dvb-t illuminators of opportunity," *IEEE Geoscience and Remote Sensing Letters*, vol. 13, no. 8, pp. 1124–1128, Aug 2016.

16. H. Zarrinkoub, *Understanding LTE with MATLAB®*, Wiley, 2014.

17. Digital Video Broadcasting, "EN 300 744 - V1.6.1 - Digital Video Broadcasting (DVB); Framing structure, channel coding and modulation for digital terrestrial television," vol. 1, pp. 1–66, 2009.

18. H. Andrew Harms, Linda M. Davis, and James Palmer, "Understanding the signal structure in DVB-T signals for passive radar detection," *IEEE National Radar Conference - Proceedings*, pp. 532–537, 2010.

19. European Telecommunications Standards Institute, "Radio Broadcasting Systems; Digital Audio Broadcasting (DAB) to mobile, portable and fixed receivers," *Technical Specification*, vol. 0, pp. 9, 2006.

20. S. Haykin, *Adaptive Filter Theory*, Prentice Hall, fourth edition, 2002.

21. K. Kulpa, M. Malanowski, P. Samczynski, and B. Dawidowicz, "The concept of airborne passive radar," *2011 Microwaves, Radar and Remote Sensing Symposium, MRRS-2011 - Proceedings*, pp. 267–270, 2011.

22. Fabiola Colone, D. W. O'Hagan, P. Lombardo, and C. J. Baker, "A multistage processing algorithm for disturbance removal and target detection in passive bistatic radar," *IEEE Transactions on Aerospace and Electronic Systems*, vol. 45, no. 2, pp. 698–722, 2009.

23. Roberta Cardinali, Fabiola Colone, Chiara Ferretti, and Pierfrancesco Lombardo, "Comparison of clutter and multipath cancellation techniques for passive radar," *IEEE National Radar Conference - Proceedings*, pp. 469–474, 2007.

24. J. L. Garry, G. E. Smith, and C. J. Baker, "Direct signal suppression schemes for passive radar," *2015 Signal Processing Symposium, SPSympo 2015*, 2015.

25. James E Palmer, H Andrew Harms, Student Member, Stephen J Searle, Linda M Davis, and Senior Member, "DVB-T Passive Radar Signal Processing," *IEEE Transactions on Signal Processing*, vol. 61, no. 8, pp. 2116–2126, 2013.

26. D. Gromek, K. Kulpa, and P. Samczyski, "Experimental results of passive sar imaging using dvb-t illuminators of opportunity," *IEEE Geoscience and Remote Sensing Letters*, vol. 13, no. 8, pp. 1124–1128, Aug 2016.

27. G. W. Stimson, D.G. Griffiths, C. J. Baker, and D. Adamy, *Introduction to Airborne Radar*, Scitech, 2014.

28. D. Astely, E. Dahlman, A. Furuskr, Y. Jading, M. Lindstrm, and S. Parkvall, "Lte: the evolution of mobile broadband," *IEEE Communications Magazine*, vol. 47, no. 4, pp. 44–51, April 2009.

29. Z. Gao, R. Tao, Y. Ma, and T. Shao, "Dvb-t signal cross-ambiguity functions improvement for passive radar," in *2006 CIE International Conference on Radar*, Oct 2006, pp. 1–4.

30. R. Saini and M. Cherniakov, "Dtv signal ambiguity function analysis for radar application," *IEE Proceedings - Radar, Sonar and Navigation*, vol. 152, no. 3, pp. 133–142, June 2005.

31. J. R. Gutierrez del Arroyo, J. A. Jackson, and M. A. Temple, "Receive signal processing for ofdm-based radar imaging," in *2013 IEEE International Conference on Acoustics, Speech and Signal Processing*, May 2013, pp. 2775–2779.

REPORT DOCUMENTATION PAGE

Form Approved
OMB No. 0704–0188

1. REPORT DATE *(DD–MM–YYYY)*	2. REPORT TYPE	3. DATES COVERED *(From — To)*
21–03–2019	Master's Thesis	Sept 2017 — Mar 2019

4. TITLE AND SUBTITLE

Direct Path Interference Suppression and Received Signal Processing for OFDM Passive Radar

5a. CONTRACT NUMBER

5b. GRANT NUMBER

5c. PROGRAM ELEMENT NUMBER

6. AUTHOR(S)

FLTLT Aileen Nundu

5d. PROJECT NUMBER

5e. TASK NUMBER

5f. WORK UNIT NUMBER

7. PERFORMING ORGANIZATION NAME(S) AND ADDRESS(ES)

Air Force Institute of Technology
Graduate School of Engineering and Management (AFIT/EN)
2950 Hobson Way
WPAFB OH 45433-7765

8. PERFORMING ORGANIZATION REPORT NUMBER

AFIT-ENG-MS-19-M-049

9. SPONSORING / MONITORING AGENCY NAME(S) AND ADDRESS(ES)

Department of Electrical Engineering
2950 Hobson Way
WPAFB OH 45433-7765
DSN 271-0690, COMM 937-255-3636
Email: julie.jackson@afit.edu

10. SPONSOR/MONITOR'S ACRONYM(S)

11. SPONSOR/MONITOR'S REPORT NUMBER(S)

12. DISTRIBUTION / AVAILABILITY STATEMENT

DISTRIBUTION STATEMENT A:
APPROVED FOR PUBLIC RELEASE; DISTRIBUTION UNLIMITED.

13. SUPPLEMENTARY NOTES

14. ABSTRACT

Passive bistatic radar (PBR) is a fairly active area of research due to the opportunities offered by the ability to use emitters of opportunity for target detection and tracking as well as Synthetic Aperture Radar (SAR) imaging. There is an increasing variety and availability of signals that can be exploited for passive radar and there is also the advantage of angular diversity offered by the bistatic geometry and the potential for stealth operations afforded a passive receiver. Notwithstanding its merits, PBR is complicated by the inevitable presence of Direct Path Interference (DPI) from the transmitter to the receiver, which can be orders of magnitude stronger than the echo signals from the targets of interest, resulting in missed targets. In addition, available signals are characterized by features necessary for the purpose for which they are designed, but that are not suited to radar applications due to the introduction of ambiguities in range and Doppler that mimic real targets. This thesis seeks to articulate two specific challenges of PBR in the context of SAR imaging using OFDM signals - DPI and range ambiguities, and the signal processing necessary to mitigate their effects. MATLAB® simulated scenarios are used throughout the work to illustrate the problem and solutions.

15. SUBJECT TERMS

Passive radar, Direct path interference suppression, OFDM passive radar, OFDM passive SAR

16. SECURITY CLASSIFICATION OF:			17. LIMITATION OF ABSTRACT	18. NUMBER OF PAGES	19a. NAME OF RESPONSIBLE PERSON
a. REPORT	b. ABSTRACT	c. THIS PAGE			Dr. J. A. Jackson, AFIT/ENG
U	U	U	UU	104	19b. TELEPHONE NUMBER *(include area code)* (937) 255-3636, x4678; julie.jackson@afit.edu